

Scalable Alignment of Process Models and Event Logs: An Approach Based on Automata and S-Components

Daniel Reißner^a, Abel Armas-Cervantes^a, Raffaele Conforti^a, Marlon Dumas^b, Dirk Fahland^c, Marcello La Rosa^a

^aUniversity of Melbourne, Australia

^bUniversity of Tartu, Estonia

^cEindhoven University of Technology, Netherlands

Abstract

Given a model of the expected behavior of a business process and given an event log recording its observed behavior, the problem of business process conformance checking is that of identifying and describing the differences between the process model and the log. A desirable feature of a conformance checking technique is that it should identify a minimal yet complete set of differences. Existing conformance checking techniques that fulfill this property exhibit limited scalability when confronted to large and complex process models and event logs. This paper presents two complementary techniques to address these shortcomings. The first technique starts by transforming the process model and the event log into two automata. These automata are then compared using an error-correcting synchronized product, computed via an A* heuristic with an admissible heuristic function, which guarantees that the resulting synchronized product captures all differences with a minimal amount of error corrections. The synchronized product is then used to extract minimal-length alignments between each trace of the log and the closest corresponding trace of the model, as well as statements describing the behavior observed in the log but not captured in the model, and vice-versa. A limitation of this first technique is that as the level of concurrency in the process model increases, the size of the automaton of the process model grows exponentially, thus hampering scalability. To address this limitation, the paper proposes a second technique wherein the process model is first decomposed into a set of automata, known as S-components, such that the product of these automata is equal to the automaton of the whole process model. An error-correcting product automaton is computed for each S-component separately and the resulting product automata are recomposed into a single error-correcting product automaton capturing all the differences between the process model and the event log, but without minimality guarantees. An empirical evaluation shows that the proposed techniques outperform state-of-the-art baselines in terms of computational efficiency. Moreover, the decomposition-based technique leads to optimal solutions for the vast majority of datasets and quasi-optimal ones for the remaining ones.

Keywords: Process Mining, Conformance Checking, Automata, Petri nets, S-components

1. Introduction

Modern information systems maintain detailed business process execution trails. For example, an enterprise resource planning system keeps records of key events related to a company's order-to-cash process, such as the receipt and confirmation of purchase orders, the delivery of products, and the creation and payment of invoices. Such records

Email addresses: dreissner@student.unimelb.edu.au (Daniel Reißner), abel.armas@unimelb.edu.au (Abel Armas-Cervantes), raffaele.conforti@unimelb.edu.au (Raffaele Conforti), marlon.dumas@ut.ee (Marlon Dumas), d.fahland@tue.nl (Dirk Fahland), marcello.larosa@unimelb.edu.au (Marcello La Rosa)

can be grouped into an *event log* consisting of sequences of events (called *traces*), each consisting of all event records pertaining to one case of a process.

Process mining techniques [1] allow us to exploit such event logs in order to gain insights into the performance and conformance of business processes. One widely used family of process mining techniques is conformance checking [2]. A conformance checking technique takes as input a process model capturing the expected behavior of a business process, and an event log capturing its observed behavior. The goal of conformance checking is to identify and describe the differences between the process model and the event log. A desirable feature of a conformance checking technique is that it should identify a minimal yet complete set of behavioral differences.

Existing conformance checking techniques that fulfill these properties [3, 4, 5] exhibit limited scalability when confronted to large and complex event logs. For example, in a collection of 40 real-life event logs presented later in this paper, the execution times of these techniques are over 10 seconds in about a quarter of cases and over 5 seconds in about half of cases, which hampers the use of these techniques in interactive settings as well as in use cases where it is necessary to apply conformance checking repeatedly, for example in the context of automated process discovery [6], where several candidate models need to be compared by computing their conformance with respect to a given log.

This paper presents two complementary techniques to address these shortcomings. The first technique starts by transforming the process model and the event log into two automata. Specifically, the process model is transformed into a minimal Deterministic Acyclic Finite State Automaton (DAFSA), while the process model is transformed into another automaton, namely its *reachability graph*. These automata are then compared using an error-correcting synchronized product, computed via an A* heuristic with an admissible heuristic function, which guarantees that the resulting synchronized product captures all differences with a minimal number of error corrections. The synchronized product is then used to extract optimal (minimal-size) alignments between each trace of the log and the closest corresponding trace of the model, as well as statements describing the behavior observed in the log but not captured in the model, and vice-versa, using the verbalization technique presented in [4].

A limitation of this first technique is that as the level of concurrency in the process model increases, the size of the automaton of the process model grows exponentially, thus hampering scalability. For example, we consider the loan application process model displayed in Fig. 1 using BPMN notation. The process starts when a credit application is received, then the credit history, the income sources, personal identification and other financial information are checked. Once the application is assessed, either a credit offer is made, the application is rejected or additional information is requested (the latter leading to a re-assessment). Note that the number of possible interleavings of the parallel activities increases rapidly, in this case the four tasks in parallel can be executed in 24 different ways, thus leading to a combinatorial explosion when computing an automaton from this process model.

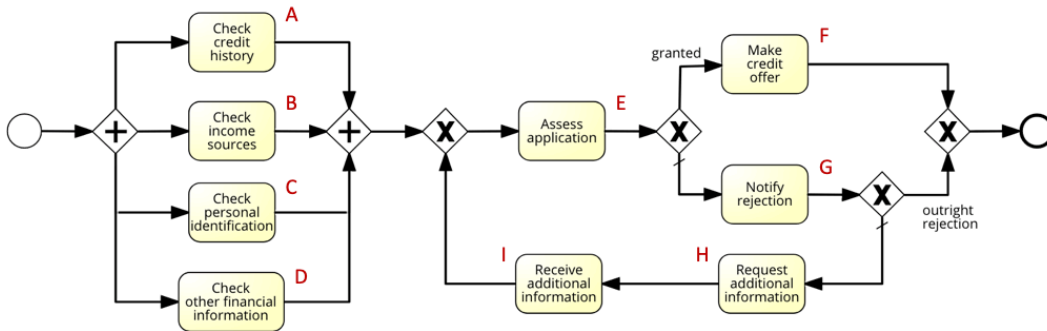


Figure 1. Example loan application process model, adapted from [4].

To address this shortcoming, the paper proposes a second technique wherein the process model is first decomposed into a set of automata, known as S-components, such that the product of these automata is equal to the automaton of the whole process model. An error-correcting product automaton is computed for each S-component separately and the resulting product automata are then recomposed into a single error-correcting product automaton capturing all the differences between the process model and the event log, but without minimality guarantees.

Coming back to the example in Fig. 1, the second technique starts by decomposing the model into four sub-models – each containing one of the four parallel tasks. Each of these concurrency-free models is then handled separately,

thus avoiding the computation of all possible interleavings and reducing the search space for computing the minimal error-correcting synchronized product.

This paper is an extended and revised version of a previous conference paper [7]. This latter paper introduced the first technique mentioned above (automata-based conformance checking). With respect to the conference version, the additional contributions are the decomposition-based technique, an extensive empirical evaluation based on 40 real-life datasets, as well as correctness proofs both for the automata-based and the decomposition-based technique.

The next section discusses existing conformance checking techniques. Section 3 introduces definitions and notations related to finite state machines, Petri nets and event logs. Next, Section 4 introduces the automata-based technique, while Section 5 presents the technique based on S-component decomposition. Finally, Section 6 presents the empirical evaluation while Section 7 summarizes the contributions and discusses avenues for future work.

2. Related Work

Conformance checking encompasses the identification of two types of discrepancies between a process model and a log: behavior observed in the log that is disallowed by the model (*unfitting behavior*), and behavior allowed by the model but not observed in the log (*additional behavior*) [4]. In this article, we focus only on detecting unfitting behavior and thus we limit the scope to this conformance dimension.

A simple approach to detect and measure unfitting behavior is *token-based replay* [8]. The idea is to replay each trace against the model. The process model is represented as a Petri net, a specific process modelling language with formal execution semantics for activities. The idea is to execute activities in the process model following the order dictated by a given trace. Whenever the process model cannot execute an activity, the technique determines the missing enabling state in the process model and *adds* a token to enable the process model to continue executing activities. Once the replay is finished, the technique counts the amount of *remaining* tokens, i.e. states during the execution of activities in the process model that were abandoned since they could not follow the order of activities of the given trace. The amount of unfitting behavior between the model and the log is then quantified in terms of the number of added and remaining tokens (replay errors). An extended version of this approach, namely *continuous semantics fitness* [9], achieves higher performance at the expense of incompleteness. Another extension [10] decomposes the model into single-entry single-exit fragments, such that each fragment can be replayed independently. Other extensions based on model decomposition are discussed in [11]. Replay fitness methods fail to identify a minimum number of errors required to explain unfitting log behavior, thus overestimating the magnitude of differences [3].

Trace alignment techniques extend replay techniques with the idea of computing an optimal (minimal-length) alignment between each trace in the log and the closest corresponding trace of the process model. In this context, an alignment of two traces is a sequence of *moves* (or *edit operations*) that describe how two cursors can move from the start of the two traces to their end. In a nutshell, there are two types of edit operations. A *match* operation indicates that the next activity is the same in both traces. Hence, the cursors can move forward by one position along both traces, simultaneously. Meanwhile, a *hide* operation (deletion of an element in one of the traces) indicates that the next activities are different in each of the two traces, or that one of the cursor has reached the end of one trace but the other cursor has not reached the end of its trace. Hence, the cursor advances along one of the traces, but not along the other. An alignment is optimal if it contains a minimal number hide operations possible.

Conformance checking techniques that produce trace alignments can be subdivided into *all-optimal* and *one-optimal*. A conformance checking technique is called *all-optimal* if it computes every possible minimal-sized alignment between each log trace and the model. Meanwhile, a conformance checking technique is called *one-optimal* if computes only one minimal-sized alignment for each log trace.

The idea of computing alignments between a process model (captured as a BPMN model) and an event log was developed in Adriansyah et al. [3]. This latter work maps each trace in the log into a (perfectly sequential) Petri net, and it then applies an A* algorithm to compute an optimal alignment between the Petri net representing the model, and the perfectly sequential net corresponding to the trace. Van Dongen [5] extends Adriansyah et al's technique [3] by strengthening the underlying heuristic function. This latter technique was shown to outperform [3] on an artificial dataset and a handful of real-life event log-model pairs. In the empirical evaluation reported later in this article, we use both [3] and [5] as baselines.

De Leoni et al [12] translate the trace alignment problem into an automated planing problem. Their argument is that a standard automated planner provides a more standardized implementation and more configuration possibilities

from the route planning domain. Depending on the planner implementation, this approach can either provide optimal or approximate solutions. In their evaluation, De Leoni et al. show that their approach can outperform [3] only on very large process models. Subsequently, [5] empirically showed that trace alignment techniques based on the A* heuristics outperform the technique of De Leoni et al. Accordingly, in this article we did not retain the technique by De Leoni et al. as a baseline.

Behavioral alignment [4] is a conformance checking technique that starts by transforming both the input event log and the process model into *event structures* [13]. It then computes a minimal error-correcting product between these two event structures. Based on this product, a set of statements are derived, which characterize all behavioral relations between tasks captured in the model but not observed in the log and vice-versa. The emphasis of behavioral alignment is on the completeness and interpretability of the set of *difference statements* that it produces. However, as shown in [4], the technique is less scalable than that of [3]. Since the emphasis of this article is on scalability, we do not retain [4] as a baseline. On the other hand, the technique proposed in this paper computes as output the same data structure as [4] (a so-called Partially Synchronized Product – PSP). Hence, the output of the techniques proposed in this article can be used to derive the same natural-language difference statements as in [4].

Sequential alignments [14] is an approximate technique that proposes an incremental approach to calculate alignments. The technique relies an ILP program to find the cheapest edit operations of the alignment for a fixed number of steps taking into account an estimate for the remaining alignment. The approach then recursively extends the found solution with another fixed number of steps until an alignment is computed. We did not consider this approach in the evaluation since the core idea of this technique was used in the extended marking equation alignment approach presented in [5] in order to derive optimal alignments with better performance. In other words, [5] subsumes [14].

Another approximate model-log alignment approach is the *evolutionary approximate alignments* [15], which aims at detecting all possible alignments with approximately optimal cost, by encoding the computation of alignments as a genetic algorithm. Tailored crossover and mutation operators are applied to an initial population of model mismatches to derive a set of alignments for each trace. In this article, we focus on computing one quasi-optimal alignment per trace (not all possible alignments) and thus we do not consider these approaches in the evaluation. Naturally, approaches that compute all-optimal alignments are slower than those that compute one-optimal alignments, and hence the comparison is unfair.

Another type of approaches focus on dividing the process model into smaller parts to speed up the computation of alignments by exploring smaller search spaces. The idea of decomposing a process model for different applications in process mining was first presented in [16]. The paper suggests a set of rules for a valid decomposition of a model to be used in conformance checking. The authors in [11] present an approach based on the decomposition of a model into *single-entry-single-exit* (SESE) fragments. The SESE approach then applies the trace alignment technique to each submodel and each trace of the event log projected onto the submodel. As a result, the technique achieves a set of decomposed alignments that can pinpoint mismatches to certain parts of the submodel. However, it does not provide complete alignments for each log trace. The SESE approach is adapted in [17] to be applicable to a specific family of models, so called *workflow nets*. The work in [18] presents an extension of [11]. This technique traverses the decomposed alignments and merge them to create an alignment. This technique sometimes computes optimal alignments, but other times it produces so-called *pseudo-alignments* – i.e., alignments that correspond to a trace in the log but not necessarily to a trace in the process model. In this article, the goal is to produce actual alignments (not pseudo-alignments). Therefore, we do not retain [18] as a baseline.

Song et al. [19] presents another approach for *recomposing alignments* that aims at closing the circle of decomposed conformance checking by proposing a procedure to re-compose the identified decomposed alignments while avoiding pseudo-alignments. Specifically, if the merging algorithm in [18] can not re-compose the decomposed alignments to an optimal one, the algorithm will merge submodels and re-compute the decomposed alignment. This procedure is repeated until the recomposition yields to an optimal alignment. A limitation of [19] is that it requires a manual model decomposition as input. The goal of the present article is to compute alignments between a log and a process model automatically, and hence we do not retain [19] as a baseline.

3. Preliminaries

This section defines the formal concepts and notations used throughout the paper: finite state machines, Petri nets and event logs. The various concepts presented herein use labelling functions to assign labels to elements. For the

sake of uniformity, L denotes a finite set of labels, τ is a special “silent” label and we write $\Sigma = L \cup \{\tau\}$. We use Z-notation [20] operators over sequences. Given a sequence $c = \langle x_1, x_2, \dots, x_n \rangle$, $|c|$ denotes the size, and $head$ and $tail$ retrieve the first and last element of a sequence, respectively, i.e., $|c| = n$, $head(c) = x_1$ and $tail(c) = x_n$. The element at index i in the sequence c is retrieved as $c[i] = x_i$. The operators *for* and *after* retrieve the elements before and after i in a sequence, respectively. For example, $for(c, i) = \langle x_1, \dots, x_i \rangle$ and $after(c, i) = \langle x_{i+1}, \dots, x_n \rangle$. Finally, *MultiSet* denotes the multiset representation of a sequence.

3.1. Finite state machines

A pervasive concept in our approaches is that of finite state machine (FSM), which is defined as follows.

Definition 3.1 (Finite State Machine (FSM)). *Given the set of labels Σ , a finite state machine is a directed graph $\mathcal{F} = (N, A, s, R)$, where N is a finite non-empty set of states, $A \subseteq N \times \Sigma \times N$ is a set of arcs, $s \in N$ is an initial state, and $R \subseteq N$ is a set of final states.*

An arc in a FSM is a triplet $a = (n_s, l, n_t)$, where n_s is the *source* state, n_t is the *target* state and l is the *label* associated to the arc. We define functions $src(a) = n_s$ to retrieve the source state, $\lambda(a) = l$ to retrieve the label and $tgt(a) = n_t$ to retrieve the target state of a . Furthermore, given a node $n \in N$ and arc $a = (n_s, l, n_t) \in A$, let $n \blacktriangleright a = n_t$ if $n = n_s$, and $n \blacktriangleright a = n$ otherwise. The set of incoming and outgoing arcs of a state n is defined as $\blacktriangleright n = \{a \in A \mid n = tgt(a)\}$ and $n \blacktriangleright = \{a \in A \mid n = src(a)\}$, respectively. Finally, a sequence of (contiguous) arcs in a FSM is called a *path*.

3.2. Petri nets

Process models are normative descriptions of business processes and define the expected behavior of the process. Over the years, several business process modelling languages have been proposed, such as Petri nets, BPMN and EPC. In the context of this work, business processes are represented as a particular family of Petri nets, namely *labelled free-choice sound workflow nets*. This formalism uses transitions to represent activities, and places to represent resource containers. The formal definition of labelled Petri nets is given next.

Definition 3.2 (Labelled Petri net). *A (labelled) Petri net, or simply a net, is the tuple $\mathcal{N} = (P, T, F, \lambda)$, where P and T are disjoint sets of places and transitions, respectively (together called nodes); $F \subseteq (P \times T) \cup (T \times P)$ is the flow relation, and $\lambda : T \rightarrow \Sigma$ is a labelling function mapping transitions to the set of task labels Σ containing the special label τ .*

Transitions labeled with τ describe invisible actions that are not recorded in the event log when executed. A node x is in the preset of a node y if there is a transition from x to y and, conversely, a node z is in the postset of y if there is a transition from y to z . Then, the preset of a node y is the set $\bullet y = \{x \in P \cup T \mid (x, y) \in F\}$ and the postset of y is the set $y \bullet = \{z \in P \cup T \mid (y, z) \in F\}$.

Workflow nets [21] are Petri nets with two special places, an initial and a final place.

Definition 3.3 (Labelled workflow net). *A (labelled) workflow net is a triplet $WN = (\mathcal{N}, i, o)$, where $\mathcal{N} = (P, T, F, \lambda)$ is a labelled Petri net, $i \in P$ is the initial and $o \in P$ is the final place, and the following properties hold:*

- The initial place i has an empty preset and the final place has an empty postset, i.e., $\bullet i = o \bullet = \emptyset$.
- If a transition t^* were added from o to i , such that $\bullet i = o \bullet = \{t^*\}$, then the resulting net is strongly connected.

The execution semantics of a net can be represented by means of markings. A marking $m : P \rightarrow \mathbb{N}_0$ is a function that associates places to natural numbers representing the amount of *tokens* in each place at a given execution state. As we will later work with the so-called incidence matrix of a Petri net, we define the semantics already in terms of vectors over places. Fixing an order $\{p_1, \dots, p_k\} = P$ over all places, we write a marking m as a column vector $m = \langle m(p_1), \dots, m(p_n) \rangle^T$. We slightly abuse notation and write m for both the function and the column vector; further we represent m as the multiset of marked places in our examples. In vector notation, the pre-set $\bullet t$ of any transition t defines a column-vector $N^-(t) = \langle x_1, \dots, x_k \rangle^T$ with $x_i = 1$ if $p_i \in \bullet t$, and $x_i = 0$ otherwise. Correspondingly, we define $N^+(t) = \langle z_1, \dots, z_k \rangle^T$ with $z_i = 1$ if $p_i \in t \bullet$, and $z_i = 0$ otherwise, for the post-set of t . We lift $+$, $-$, and \leq to vectors by element-wise application.

A transition t is *enabled* at a marking m if each pre-place of t contains a token in p , i.e., $N^-(t) \leq m$. An enabled transition t can *fire* and yield a new marking $m' = m - N^-(t) + N^+(t)$ by consuming from all its pre-places ($N^-(t)$) and producing on all its post-places ($N^+(t)$). A marking m is *reachable* from another marking m' , if there exists a sequence of firing transitions $\sigma = \langle t_1, \dots, t_n \rangle$ such that $\forall 1 \leq i < n : m_i = m_{i-1} - N^-(t_i) + N^+(t_i) \wedge N^-(t_i) \leq m_{i-1}$, where $m_0 = m'$ and $m_n = m$. A marking k -bounded if every place at a marking m has up to k tokens, i.e., $m(p) \leq k$ for any $p \in P$. A net equipped with an initial marking and a final marking is called a (Petri) *system net*. The following definition for net system refers specifically to workflow nets.

Definition 3.4 (System net). A System net SN is a triplet $SN = (WN, m_0, m_f)$, where WN is a labelled workflow net, m_0 denotes the initial marking and m_f denotes the final marking.

A system net is k -bounded if every reachable marking in the net is k -bounded. This work considers 1-bounded system nets that are *sound* [22], i.e., where from any marking m reachable from m_0 we can always reach some $m_f \in m_f$, there is no reachable marking $m > m_f \in m_f$ that contains a final marking, and each transition is enabled in some reachable marking. Figure 2 shows the system net representation for our running example.

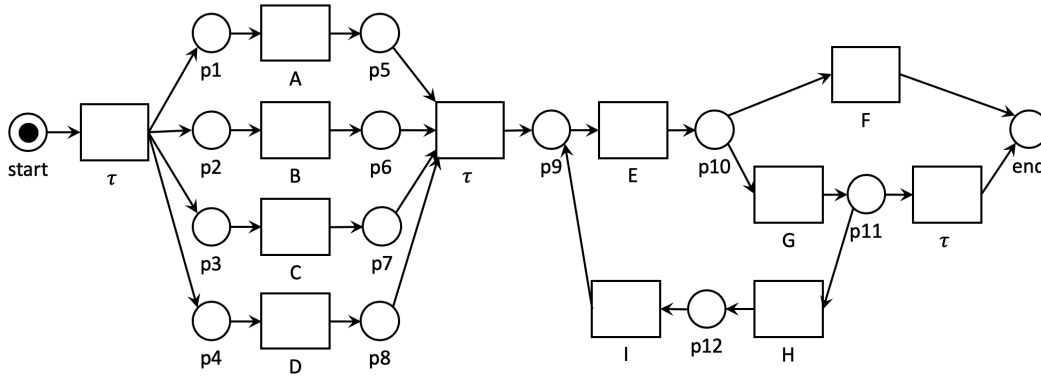


Figure 2. System net representation of the running example of Fig. 1.

The reachability graph [23] of a system net SN contains all possible markings of SN – denoted as M . Intuitively, a reachability graph is a non-deterministic FSM where states denote markings, and arcs denote the firing of a transition from one marking to another. The reachability graph for the running example is depicted in Fig. 3 showing markings as multi-sets of places. In this figure, every node contains the places with a token at each of the reachable markings. The complexity for constructing a reachability graph of a safe Petri net is $O(2^{|P \cup T|})$ [24].

Definition 3.5 (Reachability graph). The reachability graph of a System net $SN = (WN, m_0, m_f)$ is a non-deterministic finite state machine $\mathcal{R} = (M, A_{\mathcal{R}}, m_0, m_f)$, where M is the set of reachable markings and $A_{\mathcal{R}}$ is the set of arcs $\{(m_1, \lambda(t), m_2) \in M \times \Sigma \times M \mid m_2 = m_1 - \bullet t + t \bullet\}$.

3.3. Event logs

Event logs, or simply *logs*, record the execution of activities in a business process. These logs represent the executions of process instances as *traces* – sequences of activity occurrences (a.k.a. *events*). A trace can be represented as a sequence of labels, such that each label signifies an event. Although an event log is a multiset of traces containing several occurrences of the same trace, we are only interested in the distinct traces in the log and, therefore, we define a log as a set of traces. Figure 4 depicts an example of a log containing activities of the loan application process in Fig. 1 – for readability purposes, Fig. 4 uses the letters next to each of the activities in the model in Fig. 1.

Definition 3.6 (Trace and event log). Given a finite set of labels L , a trace is a finite sequence of labels $\langle l_1, \dots, l_n \rangle \in L^*$, such that $l_i \in L$ for any $1 \leq i \leq n$. An event log \mathcal{L} is a set of traces.

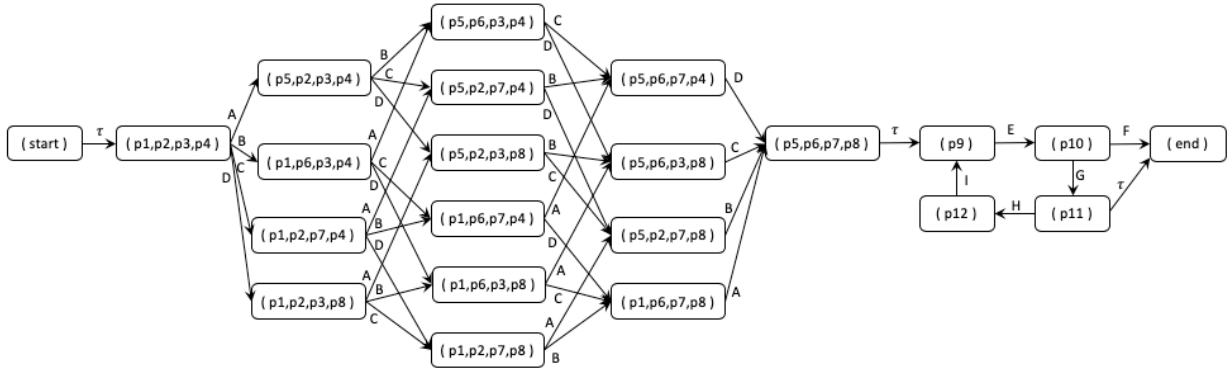


Figure 3. Reachability graph of the running example.

Log
$\langle B, D, C, E, G \rangle$
$\langle B, D, A, E, F, G \rangle$
$\langle C, A, B, E, E, G \rangle$
$\langle C, A, B, E, H, I, E, F, G \rangle$

Figure 4. Example log for our loan application process.

4. Automata-based conformance checking

The objective of conformance checking is to identify an ideally *minimal* set of differences between behavior of a given process model and a given log. As illustrated in Fig. 5, the first approach proposed in this paper does so by constructing an error-correcting product, between the reachability graph of the model and an automaton-based representation of the log (called DAFSA). (1) First, the input process model is expanded into a reachability graph. (2) In parallel, the event log is compressed into a minimal acyclic and deterministic FSM, a.k.a. DAFSA. The resulting reachability graph and DAFSA are then compared (3) to create an error-correcting synchronized product automaton – herein called a PSP, short for Partially Synchronized Product. Each state in the PSP is a pair consisting of a state in the reachability graph and a state in the DAFSA. A PSP represents a set of optimal trace alignments that can be used for (4) diagnosing behavioral difference statements via further analysis. The rest of this section starts by introducing some necessary concepts and is followed by a description of each of the steps.

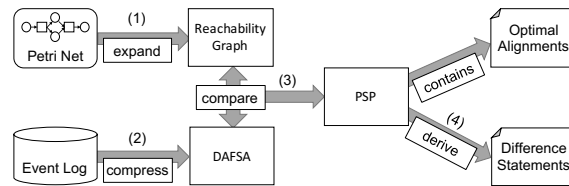


Figure 5. Overview of the automata-based approach.

4.1. τ -less reachability graph of a process model

Even though τ -transitions represent invisible steps that are not recorded in an event log, they are captured in the reachability graph of a Petri net. In principle, we assume that a Petri net has a minimal number of τ -transitions, for instance, by applying structural reduction rules that preserve all visible behavior [25]. However not all τ -transitions can be removed by structural reduction of the Petri net. We therefore remove the remaining τ -transitions through

Algorithm 1: Remove Tau Transitions

```

input: Reachability Graph  $\mathcal{R}$ 
1   $\sigma \leftarrow \langle m_0 \rangle$ ;
2   $\Omega \leftarrow \{m_0\}$ ;
3  while  $\sigma \neq \langle \rangle$  do
4     $m \leftarrow \text{head } \sigma$ ;
5     $\sigma \leftarrow \text{tail } \sigma$ ;
6     $\Psi \leftarrow \{a = (m_1, l, m) \in \blacktriangleright m \mid l = \tau \wedge m \notin m_f\}$ ;
7    for  $a \in \Psi$  do  $\text{replaceTau}(a, m, \{m\})$ ;
8     $A_{\mathcal{R}} \leftarrow A_{\mathcal{R}} \setminus \Psi$ ;
9    for  $(m, l, m_2) \in m \blacktriangleright \mid m_2 \notin \Omega$  do
10      $\sigma \leftarrow \sigma \oplus m_2$ ;
11      $\Omega \leftarrow \Omega \cup \{m_2\}$ ;
12   $\Xi \leftarrow \{m \in M \mid (\blacktriangleright m = \emptyset \wedge m \neq m_0) \vee (m \blacktriangleright = \emptyset \wedge m \notin m_f)\}$ ;
13  while  $\Xi \neq \emptyset$  do
14    for  $m \in \Xi$  do  $A \leftarrow A \setminus (\blacktriangleright m \cup m \blacktriangleright)$ ;
15     $M \leftarrow M \setminus \Xi$ ;
16     $\Xi \leftarrow \{m \in M \mid (\blacktriangleright m = \emptyset \wedge m \neq m_0) \vee (m \blacktriangleright = \emptyset \wedge m \notin m_f)\}$ ;
17  for  $a = (m_1, l, m_f) \in \blacktriangleright m_f \mid l = \tau$  do  $\text{replaceTauBackwards}(a)$ ;
18  return  $\mathcal{R}$ ;
19  Function  $\text{replaceTau}((m_1, \tau, m) \in A, m_i \in M, \Theta \in 2^M)$ 
20    for  $(m_i, l, m_2) \in m_i \blacktriangleright$  do
21      if  $l \neq \tau \vee m_2 \in m_f$  then  $A_{\mathcal{R}} \leftarrow A_{\mathcal{R}} \cup \{(m_1, l, m_2)\}$ ;
22      else if  $m_2 \notin \Theta$  then
23         $\Theta \leftarrow \Theta \cup \{m_2\}$ ;
24         $\text{replaceTau}((m_1, \tau, m), m_2, \Theta)$ ;
25  Function  $\text{replaceTauBackwards}((m_1, \tau, m_f) \in A_{\mathcal{R}})$ 
26    for  $(m_2, l, m_1) \in \blacktriangleright m_1 \mid l \neq \tau$  do  $A_{\mathcal{R}} = A_{\mathcal{R}} \cup \{(m_2, l, m_f)\}$ ;
27     $A_{\mathcal{R}} = A_{\mathcal{R}} \setminus \{(m_1, \tau, m_f)\}$ ;

```

behavior preserving reduction rules on the reachability graph by the breadth-first search algorithm given in Alg. 1. Intuitively, for every marking m reached by a τ -transition $a_1 = (m_1, \tau, m) \in A_R$ and any outgoing transition $a_2 = (m, l, m_2) \in A_R$, the algorithm replaces a_1 with $a_{12} = (m_1, l, m_2)$ (lines 6-8 and lines 19-21). This replacement is repeated until all arcs representing τ -transitions are removed. In case all incoming arcs of a state get replaced we also remove m and its outgoing arcs (Lines 12-16). Function replaceTau also handles the case of another outgoing τ -labeled transition $a_2 = (m, \tau, m_2)$ by a depth-first search along τ -transitions in A_R (lines 22-24). The algorithm then removes each remaining τ transition $a = (m_1, \tau, m_f)$ targeting the final marking while introducing new replacement arcs $a' = (m_2, l, m_f)$ for each incoming arc of m_1 , such that $(m_2, l, m_1) \in A_{\mathcal{R}}$ (Line 17 and function $\text{replaceTauBackwards}$). The reachability graph returned by Alg. 1 is now free of τ transitions. Figure 6 shows the τ -less reachability graph of the loan application process. Observe that the node $[p1, p2, p3, p4]$ is removed and its outgoing arcs are connected to the node $[start]$, and, similarly, node $[p5, p6, p7, p8]$ is removed and its incoming arcs now target the node $[p9]$ instead. In addition, the arc $([p11], \tau, [end])$ is replaced with the newly introduced arc $([p10], G, [end])$.

4.2. Compact DAFSA representation of an event log

Event logs can be represented as *Deterministic Acyclic Finite State Automata* (DAFSA), which are acyclic and deterministic FSMs. A DAFSA can represent words, in our case *traces*, in a compact manner by exploiting prefix and suffix compression.

Definition 4.1 (DAFSA). Given a finite set of labels L , a DAFSA is an acyclic and deterministic finite state machine $\mathcal{D} = (N_{\mathcal{D}}, A_{\mathcal{D}}, s_{\mathcal{D}}, R_{\mathcal{D}})$, where $N_{\mathcal{D}}$ is a finite non-empty set of states, $A_{\mathcal{D}} \subseteq N_{\mathcal{D}} \times L \times N_{\mathcal{D}}$ is a set of arcs, $s_{\mathcal{D}} \in N_{\mathcal{D}}$ is the initial state, $R_{\mathcal{D}} \subseteq N_{\mathcal{D}}$ is a set of final states.

Daciuk et al. [26] present an efficient algorithm for constructing a DAFSA from a set of words. In the constructed algorithm every word is a path from the initial to a final state and, vice versa, every path from an initial to a final state is one of the given words. We reuse this algorithm to construct a DAFSA from an event log, where the words are the set of traces. The complexity of building the DAFSA is $O(|L| \cdot \log n)$, where L is the set of distinct event labels, and n is the number of states in the DAFSA.

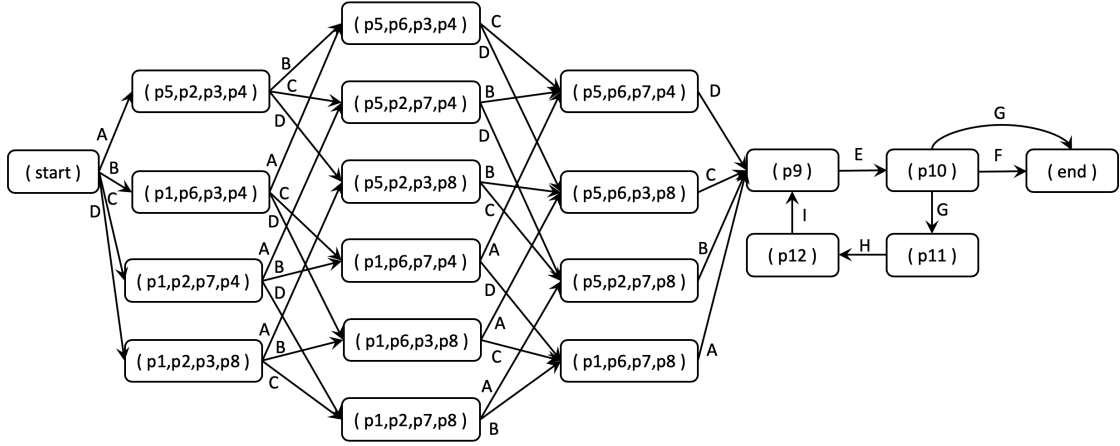


Figure 6. Tau-less reachability graph of the running example.

The *prefix* of a state $n \in N_{\mathcal{D}}$ is the sequence of labels associated to the arcs in the path from the initial state to n and, analogously, the *suffix* of n is the sequence of labels in a path from n to a final state. The prefix of the initial state and the suffix of a final state is $\{\langle \rangle\}$. A state n can have several prefixes, which are denoted by $\text{pref}(n) = \bigcup_{(n_s, l, n_t) \in \text{tr}_n} \{x \oplus l \mid x \in \text{pref}(n_s)\}$, where \oplus denotes the concatenation operator. Similarly, the set of suffixes of n is represented by $\text{suff}(n) = \bigcup_{(n_s, l, n_t) \in \text{tr}_n} \{l \oplus x \mid x \in \text{suff}(n_t)\}$. Prefixes and suffixes are said to be *common* iff they are shared by more than one trace.

Definition 4.2 (Common prefixes and suffixes). Let $\mathcal{D} = (N_{\mathcal{D}}, A_{\mathcal{D}}, s_{\mathcal{D}}, R_{\mathcal{D}})$ be a DAFSA. The set of common prefixes of \mathcal{D} is the set $\mathcal{P} = \{\text{pref}(n) \mid n \in N_{\mathcal{D}} \wedge |\text{tr}_n| > 1\}$. The set of common suffixes of \mathcal{D} is the set $\mathcal{S} = \{\text{suff}(n) \mid n \in N_{\mathcal{D}} \wedge |\text{tr}_n| > 1\}$.

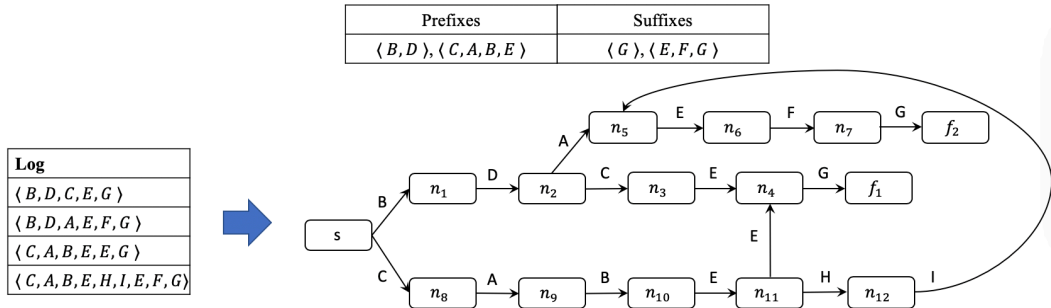


Figure 7. DAFSA representation of the running example log.

Figure 7 depicts the DAFSA representation and its corresponding common prefixes and suffixes for the example event log in Fig. 4. In total, it summarizes 26 events with 16 arcs. All traces in the event log are paths from s to one of the two final nodes f_1 or f_2 . For instance, the trace $\langle B, D, C, E, G \rangle$ is represented by the path $\langle (s, B, n_1), (n_1, D, n_2), (n_2, C, n_3), (n_3, E, n_4), (n_4, G, f_1) \rangle$. In this example, the two common prefixes in nodes n_2 and n_{11} , as well as the common suffixes from nodes n_4 and n_5 , are shared by two traces in the event log.

4.3. Error-correcting synchronised product

The computation of similar and deviant behavior between an event log and a process model is based on an error-correcting synchronized product (PSP) [27]. Intuitively, the traces represented in the DAFSA are “aligned” with the executions of the model by means of three operations: (1) synchronized move (*match*), the process model and the event log can execute the same task/event with respect to their label; (2) log operation (*lhide*), an event observed in the log cannot occur in the model; and (3) model operation (*rhide*), a task in the model can occur, but the corresponding

event is missing in the log. Both a trace in a log and an execution represented in a reachability graph are totally ordered sets of events (sequences). An alignment aims at *matching* events from both sequences that represent the tasks with the same labels, such that the order between the matched events is preserved. An event that is not matched has to be hidden using the operation *lhide* if it belongs to the log, or *rhide* if it belongs to an execution in the model. For example, given a trace in a log $\langle D, B, C, E, G \rangle$ and an execution in a model $\langle B, D, C, A, E, G \rangle$, it is possible to match the events with label *E*, and either the events with label *B* or the events with label *D*, but not both. Finally, the events that are not matched needed to be hidden.

In our context, the alignments are computed over a pair of FSMs, a DAFSA and a reachability graph, therefore the three operations: *match*, *lhide* and *rhide*, are applied over the arcs of both FSMs. A *match* is applied over a pair of arcs (one in the DAFSA and one in the reachability graph) whereas *lhide* and *rhide* are applied only over one arc. We record the type of operation and the involved arcs in a triplet called *synchronization* where \perp denotes the absence of an arc in case of *lhide* and *rhide*.

Definition 4.3 (Synchronization). *Let $\mathcal{D} = (N_{\mathcal{D}}, A_{\mathcal{D}}, s_{\mathcal{D}}, R_{\mathcal{D}})$ and $\mathcal{R} = (M, A_{\mathcal{R}}, m_0, m_f)$ be a DAFSA and a reachability graph, respectively. Then, the set of all possible synchronizations are defined as $S(\mathcal{D}, \mathcal{R}) = \{(lhide, a_{\mathcal{D}}, \perp) \mid a_{\mathcal{D}} \in A_{\mathcal{D}}\} \cup \{(rhide, \perp, a_{\mathcal{R}}) \mid a_{\mathcal{R}} \in A_{\mathcal{R}}\} \cup \{(match, a_{\mathcal{D}}, a_{\mathcal{R}}) \mid a_{\mathcal{D}} \in A_{\mathcal{D}} \wedge a_{\mathcal{R}} \in A_{\mathcal{R}} \wedge \lambda(a_{\mathcal{D}}) = \lambda(a_{\mathcal{R}})\}$.*

Given a synchronization $\beta = (op, a_{\mathcal{D}}, a_{\mathcal{R}})$, let $\beta^\ell = \lambda(a_{\mathcal{D}})$ if $a_{\mathcal{D}} \neq \perp$ and $\beta^\ell = \lambda(a_{\mathcal{R}})$ if $a_{\mathcal{R}} \neq \perp$; this notation is well-defined as $\lambda(a_{\mathcal{D}}) = \lambda(a_{\mathcal{R}})$ whenever $a_{\mathcal{D}} \neq \perp \neq a_{\mathcal{R}}$. Further, let $\beta^{op} = op$, $\beta^{a_{\mathcal{D}}} = a_{\mathcal{D}}$, and $\beta^{a_{\mathcal{R}}} = a_{\mathcal{R}}$.

All possible alignments between the traces represented in a DAFSA and the executions represented in a reachability graph can be inductively computed as follows. The construction starts by pairing the initial states of both FSMs and then applying the three defined operations over the arcs that can be taken in the DAFSA and in the reachability graph – each application of the operations (synchronization) yield a new pairing of states. Note that the alignments between (partial) traces and executions are implicitly computed as sequences of synchronizations.

Given a sequence of synchronizations $\varepsilon = \langle \beta_1, \dots, \beta_m \rangle$ with $\beta_i = (op_i, a_{i,\mathcal{D}}, a_{i,\mathcal{R}})$, $1 \leq i \leq m$, we define two projection operations $\varepsilon \upharpoonright_{\mathcal{D}}$ and $\varepsilon \upharpoonright_{\mathcal{R}}$ that retrieve the sequence of arcs for the DAFSA and the reachability graph, respectively. The *projection* onto \mathcal{D} is the sequence $\varepsilon \upharpoonright_{\mathcal{D}} = \langle a_{1,\mathcal{D}}, \dots, a_{m,\mathcal{D}} \rangle \upharpoonright_{A_{\mathcal{D}}}$ of the \mathcal{D} -entries in ε projected onto the arcs in \mathcal{D} (i.e., removing all \perp). Correspondingly, $\varepsilon \upharpoonright_{\mathcal{R}} = \langle a_{1,\mathcal{R}}, \dots, a_{m,\mathcal{R}} \rangle \upharpoonright_{A_{\mathcal{R}}}$. Thus, $\varepsilon \upharpoonright_{\mathcal{D}}$ ($\varepsilon \upharpoonright_{\mathcal{R}}$) contains the arcs of all *match* and *lhide* (*rhide*) triplets. On top of that notation, we are interested in the sequence of labels represented by a sequence of arcs, shorthand as $\lambda(\varepsilon \upharpoonright_{\mathcal{D}}) = \langle \lambda(a_1), \dots, \lambda(a_n) \rangle$.

Definition 4.4 ((Proper) Alignment). *Given a DAFSA \mathcal{D} , a reachability graph \mathcal{R} and a trace $c \in \mathcal{L}$, an alignment is defined as a sequence of synchronizations $\varepsilon_c = \langle \beta_1, \beta_2, \dots, \beta_m \rangle$, where $\beta_i \in S(\mathcal{D}, \mathcal{R}) \wedge 1 \leq i \leq |\varepsilon_c| \leq m$. A proper alignment for the trace c fulfils two properties:*

1. *The sequence of synchronizations with *lhide* or *match* operations reflects the trace c , i.e. $\lambda(\varepsilon_c \upharpoonright_{\mathcal{D}}) = c$.*
2. *The arcs of the reachability graph in the sequence of synchronizations with *rhide* or *match* operations forms a path in the reachability graph from the initial to the final marking, i.e. let $n = |\varepsilon_c \upharpoonright_{\mathcal{R}}|$, then $\text{src}(\varepsilon_c \upharpoonright_{\mathcal{R}}[1]) = m_0 \wedge \text{tgt}(\varepsilon_c \upharpoonright_{\mathcal{R}}[n]) = m_f \wedge \forall i < n : \text{tgt}(\varepsilon_c \upharpoonright_{\mathcal{R}}[i]) = \text{src}(\varepsilon_c \upharpoonright_{\mathcal{R}}[i+1])$.*

The set of all proper alignments for a given trace c is denoted as $\mathcal{C}(c, \mathcal{R})$. We write $\varepsilon_{c|op} = \{\beta = (op, a_{\mathcal{D}}, a_{\mathcal{R}}) \in \varepsilon_c\}$ for the synchronizations of a particular operation op in a given alignment ε_c .

A cost can be associated to a proper alignment for a given trace. If an asynchronous *lhide* or *rhide* move is associated to a non- τ label then the cost increases. Assuming that the cost of hiding a non- τ transition is 1, the cost function is given as follows:

Definition 4.5 (Alignment cost function). *Given an alignment $\varepsilon \in \mathcal{C}(c, \mathcal{R})$, the cost function $\text{cost} : \mathcal{C}(c, \mathcal{R}) \rightarrow \mathbb{N}$ for ε is defined as $\text{cost}(\varepsilon) = |\{\beta \in \varepsilon \mid \beta^\ell \neq \tau \wedge \beta^{op} \neq \text{match}\}|$.*

All alignments can be collected in a finite state machine called PSP [27]. Every state in the PSP is a triplet (n, m, ε) , where n is a state in the DAFSA \mathcal{D} , m is a state in the reachability graph \mathcal{R} and ε is the sequences of arcs taken in the \mathcal{D} and in \mathcal{R} to reach n and m ; every arc of the PSP is a synchronization of \mathcal{D} and \mathcal{R} ; the pairing of the initial states is the initial state of the PSP; and the final states are those with no outgoing arcs.

Definition 4.6 (PSP). *Given a DAFSA \mathcal{D} and a reachability graph \mathcal{R} , their PSP \mathcal{P} is a finite state machine $\mathcal{P} = (N_{\mathcal{P}}, A_{\mathcal{P}}, s_{\mathcal{P}}, R_{\mathcal{P}})$, where $N_{\mathcal{P}} \subseteq N_{\mathcal{D}} \times M \times \mathcal{C}$ is the set of nodes, $A_{\mathcal{P}} = N_{\mathcal{D}} \times S(\mathcal{D}, \mathcal{R}) \times N_{\mathcal{D}}$ is the set of arcs, $s_{\mathcal{P}} = (s_{\mathcal{D}}, m_0, \langle \rangle) \in N_{\mathcal{P}}$ is the initial node, and $R_{\mathcal{P}} = \{f \in N_{\mathcal{P}} \mid f \blacktriangleright = \emptyset\}$ is the set of final nodes.*

Algorithm 2: Construct the PSP

input: Event Log \mathcal{L} , DAFSA \mathcal{D} , Reachability Graph \mathcal{R} ,

```

1  for  $c \in \mathcal{L}$  do
2     $\sigma \leftarrow \{(s_{\mathcal{D}}, \rho(s_{\mathcal{D}}, c))\}$ ;
3     $\rho_{\max} \leftarrow |c| + \text{minModelSkips}$ ;
4    while  $\sigma \neq \emptyset$  do
5      choose a tuple  $(n_{act} = (n_{\mathcal{D}}, m, \varepsilon), \rho) \in \sigma$ , such that  $\nexists (n'_{\mathcal{D}}, \rho') \in \sigma : \rho > \rho'$ ;
6       $\sigma \leftarrow \sigma \setminus \{(n_{act}, \rho)\}$ ;
7      if  $n_{\mathcal{D}} \in R_{\mathcal{D}} \wedge m \in M_f \wedge \varepsilon \upharpoonright_{\mathcal{D}} = c$  then
8        if  $\rho(n_{act}, c) < \rho_{\max}$  then
9           $\rho_{\max} \leftarrow \rho(n_{act}, c)$ ;
10          $Opt \leftarrow \emptyset$ ;
11          $\sigma \leftarrow \{(n, \rho(n, c)) \in \sigma \mid \rho(n, c) \leq \rho_{\max}\}$ 
12        $Opt \leftarrow Opt \cup \{n_{act}\}$ ;
13     else
14        $N_{new} \leftarrow \emptyset$ ;
15       for  $\alpha_{\mathcal{D}} = (n_{\mathcal{D}}, l_{\mathcal{D}}, n_t) \in n_{\mathcal{D}} \blacktriangleright \mid l_{\mathcal{D}} = c(|\varepsilon \upharpoonright_{\mathcal{D}}| + 1)$  do
16          $N_{new} \leftarrow N_{new} \cup \{(n_t, m, \varepsilon \oplus (l_{hide}, \alpha_{\mathcal{D}}, \perp))\}$ ;
17         for  $\alpha_{\mathcal{R}} = (m, l_{\mathcal{R}}, m_t) \in m \blacktriangleright \mid l_{\mathcal{R}} = l_{\mathcal{D}}$  do
18            $N_{new} \leftarrow N_{new} \cup \{(n_t, m_t, \varepsilon \oplus (match, \alpha_{\mathcal{D}}, \alpha_{\mathcal{R}}))\}$ 
19       for  $\alpha_{\mathcal{R}} = (m, l_{\mathcal{R}}, m_t) \in m \blacktriangleright$  do  $N_{new} \leftarrow N_{new} \cup \{(n_{\mathcal{D}}, m_t, \varepsilon \oplus (rhide, \perp, \alpha_{\mathcal{R}}))\}$ ;
20        $\sigma \leftarrow \sigma \cup \{(n_{next}, \rho(n_{next}, c)) \mid n_{next} \in N_{new} \wedge \rho(n_{next}, c) \leq \rho_{\max}\}$ ;
21   for  $f \in Opt$  do  $InsertIntoPSP(f, c, \mathcal{P})$ ;
22 return  $\mathcal{P}$ ;

```

The PSP contains all possible alignments, however we are interested in the proper alignments with minimum cost. These alignments are called *optimal*. The computation of all possible alignments can become infeasible when the search space is too large. Thus, we use an A^* algorithm [28] to consider the most promising paths in the PSP first, i.e., those minimizing the number of hides. We define the cost function for the A^* as follows.

Definition 4.7 (A^* -cost function). *Let \mathcal{L} and \mathcal{P} be a given event log and PSP, then for every trace $c \in \mathcal{L}$ and every node $x = (n, m, \varepsilon) \in \mathcal{P}$ we define a cost function $\rho(x, c) = g(x, c) + h(x, c)$ that relies on the current cost function g and a heuristic function h for estimating future hides for a given trace. We define functions g and h as follows:*

$$g(x, c) = \begin{cases} \text{cost}(\varepsilon(x)), & \text{if } \varepsilon(x) \upharpoonright_{\mathcal{D}} = \text{for}(c, |\varepsilon(x) \upharpoonright_{\mathcal{D}}|) \\ \infty, & \text{otherwise} \end{cases} \quad (1)$$

$$h(x, c) = \min\{|F_{Log}(x, c) \setminus f_{Model}| + |f_{Model} \setminus F_{Log}(x, c)| \mid f_{Model} \in F_{Model}(x)\}$$

Function g returns the current cost for a given node x in the PSP and a given trace c to align. If the trace labels of the partial alignment of x , i.e. $\varepsilon(x) \upharpoonright_{\mathcal{D}}$, fully represent a prefix of c then the cost of $\varepsilon(x)$ is that of the *cost* function defined in Def. 4.5. Otherwise, node x is not relevant to trace c and the cost is set to ∞ to avoid considering this node in the search. Function h relies on two functions F_{Log} and F_{Model} . $F_{Log}(x, c) = \text{MultiSet}(c) \setminus \varepsilon \upharpoonright_{\mathcal{D}}$ denotes the multiset of future trace labels and F_{Model} is the set of multisets of future model labels. The set of future model labels $F_{Model}(x)$ is computed in a backwards breadth-first traversal over the strongly connected components of the reachability graph from each of its final markings. The multisets of task labels are collected during the traversal and stored in each node of the graph. All labels from cyclic arcs inside strongly connected components are gathered during the traversal with a special symbol ω representing that the label can be repeated any number of times. For the comparison of these labels to achieve an underestimating function, we set these labels to infinity for the term $|F_{Log} \setminus f_{Model}|$ and to 0 for the term $|f_{Model} \setminus F_{Log}|$, i.e. we assume that repeated task labels match all corresponding labels in the trace. Observe that h assumes that all events with the same label in F_{Log} and f_{Model} are matched, this is clearly an optimistic approximation, since some of the those matches might not be possible; then the optimistic approximation computed by h guarantees the optimality of the alignments; h is admissible.

Algorithm 2 shows the procedure to build the PSP, where an A^* search is applied to find all optimal alignments for each trace in a log. The algorithm chooses a node with minimal cost ρ , such that if it pairs two final states (one in the DAFSA and one in the reachability graph) – representing the alignment of a complete trace – then it is marked as an optimal alignment. Otherwise, the search continues by applying *lhide*, *rhide* and *match*. As shown in [4], the

Algorithm 3: Construct the PSP with Prefix- and Suffix Memoization

▷ replace line 2 with the following block:

```

▷ Reuse common prefix alignments
for  $i = 1 \rightarrow |c|$  do  $\sigma \leftarrow \sigma \cup \{(n_{next}, \rho(n_{next}, c)) \mid n_{next} \in PrefixTable(c \text{ for } i)\}$ ;
if  $\sigma = \emptyset$  then  $\sigma \leftarrow \sigma \cup \{(s_{\mathcal{D}}, \rho(s_{\mathcal{D}}, c))\}$ ;

```

▷ replace line 14 with the following block:

```

▷ Reuse common suffix alignments
 $suff_{act} \leftarrow c$  after  $\{\beta = (op, a_{\mathcal{D}}, a_{\mathcal{R}}) \in \mathcal{E} \mid op \neq rhide\}$ 
;  $N_{new} \leftarrow \{(f_{\mathcal{D}}, f_{\mathcal{R}}, \mathcal{E} \oplus g_{suff}) \mid (f_{\mathcal{D}}, f_{\mathcal{R}}, g_{suff}) \in SuffixTable(n_{\mathcal{D}}, m, suff_{act})\}$ ;
 $\sigma \leftarrow \sigma \cup \{(n_{next}, \rho(n_{next}, c)) \mid n_{next} \in N_{new}\}$ ;
if  $N_{new} \neq \emptyset$  then continue;

```

complexity for constructing the PSP is in the order of $O(3^{|N_{\mathcal{D}}| \cdot |M|})$ where $N_{\mathcal{D}}$ is the set of states in the DAFSA and M is the set of reachable markings of the Petri net.

In order to optimize the computation of the PSP, two memoization tables are used: prefix and suffix. Both tables store partial trace alignments for common prefixes and suffixes that have been aligned previously. The integration of these tables requires the modification of Alg. 2, as shown in Alg. 3. For each trace c , the algorithm starts by checking if there is a common prefix for c in the prefix memoization table. If this is the case, the A^* starts from the nodes stored in the memoization table for the partial trace alignments that have been previously observed. In the case of common suffix memoization, the algorithm checks at each iteration whether the current pair of nodes and the current suffix is stored in the suffix memoization table. If this is the case, the algorithm appends nodes to the A^* search for each pair of memoized final nodes and appends all partial suffix alignments to the current alignment instead of continuing the regular search procedure. By reusing the information stored in these tables, the search space for the A^* is reduced.

The approach illustrated so far produces a PSP containing all optimal alignments. Nevertheless, if only one optimal alignment is required, then the algorithm can be easily modified to stop as soon as the first alignment is found. Overall, the complexity of the proposed approach is exponential in the worst case, i.e. $O(|\Sigma| \cdot \log n + 2^{|P \cup T|} + 3^{|N_{\mathcal{D}}| \cdot |M|})$.

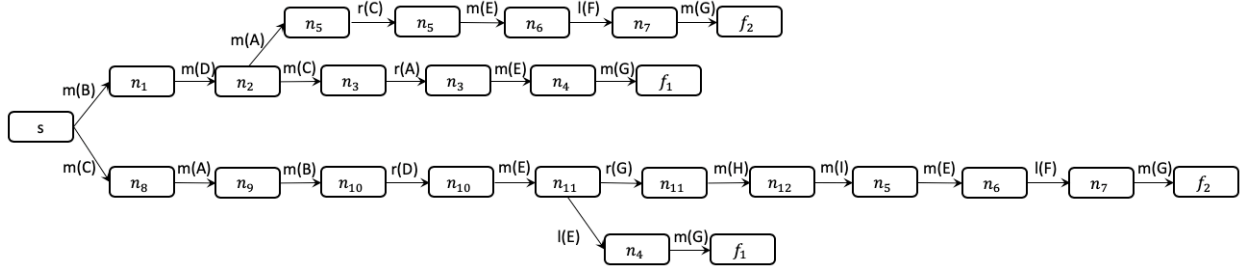


Figure 8. The PSP for our loan application process example.

Figure 8 shows an abbreviated PSP obtained by synchronizing the DAFSA of the loan application process in Fig. 7 and the τ -less reachability graph of Fig. 6. The PSP shows the one-optimal alignments and abbreviates states in the PSP with only states in the DAFSA for readability purposes, and the name of the operations are shorthanded with the initial letter and the label of the activity, i.e., $(match, x) = m(x)$. To understand its construction let us consider the sample trace $\langle B, D, C, E, G \rangle$. Starting from the source node s , $g(n) = 0$, $F_{Log}(n, c) = \{B^1, D^1, C^1, E^1, G^1\}$, and $F_{Model}(n) = \{A^1, B^1, C^1, D^1, E^1\}$. The A^* will compute the cost of performing the following possible synchronizations: $(match, B)$, $(lhide, B)$, $(rhide, A)$, $(rhide, B)$, $(rhide, C)$ and $(rhide, D)$. Out of these six possibilities it will only explore $(match, B)$ ¹ and $(rhide, A)$ which have a cost of one. Other synchronizations like $(rhide, B)$ ² will never be explored

¹In case of $(match, B)$ we have a current cost of zero since it is a match (i.e. $g(n) = 0$), and a future cost of one (i.e. $h(n, c) = |\{C^1, D^1, E^1, G^1\} \setminus \{A^1, C^1, D^1, E^1, G^1\}| + |\{A^1, C^1, D^1, E^1, G^1\} \setminus \{C^1, D^1, E^1, G^1\}| = 1)$.

²In case of $(rhide, B)$ we have a current cost of one since it is a hide (i.e. $g(n) = 1$), and a future cost of three (i.e. $h(n, c) = |\{B^1, C^1, D^1, E^1, G^1\} \setminus \{A^1, C^1, D^1, E^1, G^1\}| + |\{A^1, C^1, D^1, E^1, G^1\} \setminus \{B^1, C^1, D^1, E^1, G^1\}| = 2)$.

since they have a cost of three and there exist nodes with a lower cost. The A^* search will continue exploring the possible synchronizations until all optimal alignments are discovered.

4.4. Deterministic alignments

A trace can have several optimal alignments, however, in order to have a deterministic computation of a single optimal alignment, we define an order on the construction of the PSP. This order is imposed on the operations, with the following precedence order: $match > rhide > lhide$, and on the lexicographic order of the activity labels. We apply this precedence order at each iteration of the A^* -search on the set of candidate nodes of the queue that all have the lowest cost values w.r.t. ρ . In that way the A^* search will still always explore the cheapest nodes first and guarantees to find an alignment with optimal cost. The precedence order merely provides a tool to deterministically select an optimal alignment from the set of optimal alignments with a specific order of operations and activity labels already during the exploration of the search space.

We choose to prioritize $rhide$ over $lhide$ synchronizations in the preference order to increase the number of $match$ synchronizations in the returned optimal alignment. We would like to remind the reader that an increase in $match$ synchronizations does not change the cost function for an alignment as per Def. 4.7. An alignment with more $match$ synchronizations, however, can link the observed trace more closely to the process model. The following lemma shows that for optimal alignments, more $rhide$ synchronizations lead to more $match$ synchronizations.

Lemma 4.1. *Let ϵ_c be an optimal alignment for a trace c . For any other optimal alignment ϵ'_c for c , such that $\epsilon'_{c|rhide} < \epsilon_{c|rhide}$, then $\epsilon'_{c|match} < \epsilon_{c|match}$.*

Proof. Given two optimal alignments ϵ_c, ϵ'_c , it holds that these two alignments have the same cost according to Def. 4.5, i.e. $cost(\epsilon_c) = cost(\epsilon'_c)$, and these two alignments are proper according to Def. 4.4. Further, we assume that ϵ_c has more $rhide$ synchronizations than ϵ'_c , i.e. $\epsilon'_{c|rhide} < \epsilon_{c|rhide}$. As a first step, we assume that ϵ_c has exactly one more $rhide$ synchronization than ϵ'_c , i.e. $\epsilon_{c|rhide} = \epsilon'_{c|rhide} + 1$. The cost of an alignment is the number of $rhide$ and $lhide$ synchronizations disregarding all synchronizations involving τ . Since we remove all τ -labelled transitions in Alg. 1, the cost of an alignment equals exactly to the number of $rhide$ and $lhide$ synchronizations. By the assumptions, ϵ_c has one more $rhide$ synchronization than, and the same cost as, ϵ'_c and so it follows that ϵ'_c has exactly one more $lhide$ synchronization for a trace label ℓ than ϵ_c , i.e. $(lhide, \ell) \in \epsilon'_c \wedge (lhide, \ell) \notin \epsilon_c \wedge \ell \in c$. Since both alignments properly represent the trace, the sum of their $lhide$ and $match$ synchronizations is equal to the size of the trace $|c|$. Therefore, ϵ_c needs to have one more $match$ synchronizations than ϵ'_c , in particular $(match, \ell) \in \epsilon_c \wedge (match, \ell) \notin \epsilon'_c \wedge \ell \in c$. The general case of multiple $rhide$ synchronizations follows from inductive reasoning. If an optimal alignment ϵ_c has x more $rhide$ than another optimal alignment ϵ'_c , then ϵ'_c must have x more $lhide$ than ϵ_c because they have the same cost. Similarly, ϵ_c must have x more $match$ synchronizations than ϵ'_c since the number of $lhide$ and $match$ synchronizations needs to equal to the size of the trace $|c|$. Hence, it holds for two optimal alignments ϵ_c, ϵ'_c with $\epsilon'_{c|rhide} < \epsilon_{c|rhide}$ that $\epsilon'_{c|match} < \epsilon_{c|match}$ and thus the proof is complete. \square

Fig. 9 demonstrates all 4 possible optimal alignments with the same cost for trace $\langle B, D, C, E, G \rangle$ of the loan application example with one mismatch (missing activity A in the parallel block). Out of these four, we select alignment $\langle m(B), m(D), m(C), r(A), m(E), m(G) \rangle$ according to the precedence order.

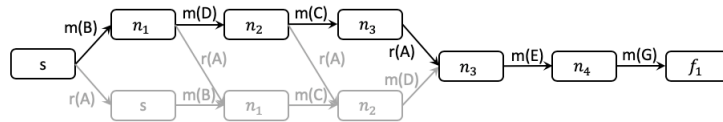


Figure 9. Deterministic one-optimal alignment for trace $\langle B, D, C, E, G \rangle$.

Algorithm 4 shows the modified procedure to construct a PSP containing one deterministic optimal alignment for a given trace c which differs from Alg. 2 by using the deterministic selection criteria explained above (line 10), and terminating when the entire trace has been read and the final state in \mathcal{R} has been reached (line 13).

Algorithm 4: Revised for one-optimal: Construct the PSP

```

input: Event Log  $\mathcal{L}$ , DAFSA  $\mathcal{D}$ , Reachability Graph  $\mathcal{R}$ 
1 for  $c \in \mathcal{L}$  do
2    $f \leftarrow \text{align}(c, \mathcal{D}, \mathcal{R})$ ;
3    $\text{InsertIntoPSP}(f, c, \mathcal{P})$ ;
4 return  $\mathcal{P}$ ;
5 Function  $\text{align}(c, \mathcal{D}, \mathcal{R})$ 
6    $\sigma \leftarrow \{(s_{\mathcal{D}}, \rho(s_{\mathcal{D}}, c))\}$ ;
7    $\rho_{\max} \leftarrow |c| + \text{minModelSkips}$ ;
8   while  $\sigma \neq \emptyset$  do
9      $\text{Opt} \leftarrow \{(n_{\mathcal{D}}, m, \varepsilon, \rho) \in \sigma, \text{ such that } \nexists (n'_{\mathcal{D}}, \rho') \in \sigma : \rho > \rho'\}$ ;
10    choose a tuple  $n_{\text{act}} = ((n_{\mathcal{D}}, m, \varepsilon), \rho) \in \text{Opt}$  with the following priorities :  $op(\varepsilon(|\varepsilon|)) : \text{match} > \text{rhide} > \text{lhide}$  and choosing  $\lambda(\varepsilon(|\varepsilon|))$  in
    lexicographical order;
11     $\sigma \leftarrow \sigma \setminus \{(n_{\text{act}}, \rho)\}$ ;
12    if  $n_{\mathcal{D}} \in R_{\mathcal{D}} \wedge m \in R_{\mathcal{R}} \wedge \varepsilon \upharpoonright_{\mathcal{D}} = c$  then
13      return  $n_{\text{act}} = (r_{\mathcal{D}}, r_{\mathcal{R}}, \varepsilon_c)$ ;
14    else
15       $N_{\text{new}} \leftarrow \emptyset$ ;
16      for  $\alpha_{\mathcal{D}} = (n_{\mathcal{D}}, l_{\mathcal{D}}, n_t) \in n_{\mathcal{D}} \blacktriangleright |l_{\mathcal{D}} = c(|\varepsilon \upharpoonright_{\mathcal{D}}| + 1)$  do
17         $N_{\text{new}} \leftarrow N_{\text{new}} \cup \{(n_t, m, \varepsilon \oplus (\text{lhide}, \alpha_{\mathcal{D}}, \perp))\}$ ;
18        for  $\alpha_{\mathcal{R}} = (m, l_{\mathcal{R}}, m_t) \in m \blacktriangleright |l_{\mathcal{R}} = l_{\mathcal{D}}$  do
19           $N_{\text{new}} \leftarrow N_{\text{new}} \cup \{(n_t, m_t, \varepsilon \oplus (\text{match}, \alpha_{\mathcal{D}}, \alpha_{\mathcal{R}}))\}$ 
20      for  $\alpha_{\mathcal{R}} = (m, l_{\mathcal{R}}, m_t) \in m \blacktriangleright$  do  $N_{\text{new}} \leftarrow N_{\text{new}} \cup \{(n_{\mathcal{D}}, m_t, \varepsilon \oplus (\text{rhide}, \perp, \alpha_{\mathcal{R}}))\}$ ;
21       $\sigma \leftarrow \sigma \cup \{(n_{\text{next}}, \rho(n_{\text{next}}, c)) \mid n_{\text{next}} \in N_{\text{new}} \wedge \rho(n_{\text{next}}, c) \leq \rho_{\max}\}$ ;

```

Note that the “final” node $(r_{\mathcal{D}}, r_{\mathcal{R}}, \varepsilon_c)$ returned in line 13 defines a sequence ε_c of synchronizations. Next, we show that ε_c is indeed an optimal alignment of c to \mathcal{R} . Let $\phi(c, \mathcal{P}) = \varepsilon_c$ be a function that “extracts” ε_c out of the constructed PSP \mathcal{P} returned by Alg. 4.

Lemma 4.2. *Let \mathcal{L} , \mathcal{D} and \mathcal{R} be an event log, a DAFSA and a reachability graph, respectively. For each trace $c \in \mathcal{L}$ and $\mathcal{P} = \text{Alg4}(\mathcal{L}, \mathcal{D}, \mathcal{R})$, it holds that $\varepsilon_c = \phi(c, \mathcal{P})$ is a proper alignment of c to \mathcal{R} , i.e. $\varepsilon_c \in \mathcal{C}(c, \mathcal{R})$.*

Proof (Sketch). In order to prove that ε_c is a proper alignment, we proceed to show that it fulfils the two properties in Def. 4.4.

(1) The projection on the DAFSA reflects the trace $\lambda(\varepsilon_c \upharpoonright_{\mathcal{D}}) = c$. Recall that the projection of any proper alignment onto \mathcal{D} contains only *match* or *lhide* operations. Alg.4 starts at the initial state of the DAFSA for every given trace, iterates over the trace (9-21) and adds *lhide*-operations (line 17) and *match*-operations (line 19) for outgoing arcs with the next label of the trace. Every alignment ε_c returned by Alg. 4 then fulfils this property by construction as it needs to fulfil the condition $\varepsilon \upharpoonright_{\mathcal{D}} = c$ in line 12 for determining if a given alignment is final.

(2) $\varepsilon_c \upharpoonright_{\mathcal{R}}$ is a path from m_0 to a final marking $m_f \in M_f$. Recall that the projection of any proper alignment onto \mathcal{R} contains only *match* or *rhide* operations. The algorithm always starts to add arcs from the initial marking of the reachability graph. At every iteration of the main loop (9-21) it either adds arcs with *match* operations in line 19 or with *rhide* operations in line 20 from the set of outgoing arcs of the current marking in the reachability graph. The algorithm then adds a new node to the queue that contains the target of the added arc. By lines 18 and 20, subsequent arcs are only added if they are outgoing arcs of the node m reached in \mathcal{R} , and thus will always form a path in \mathcal{R} . This path will always start from the initial marking and end in a final marking as per the condition in line 12 and thus it is a path through the reachability graph. \square

Lemma 4.3. *Let \mathcal{L} , \mathcal{D} and \mathcal{R} be an Event log, a DAFSA and a Reachability Graph, respectively. Then it holds for each trace $c \in \mathcal{L}$ and $\mathcal{P} = \text{Alg4}(\mathcal{L}, \mathcal{D}, \mathcal{R})$ that the alignment $\varepsilon_c = \phi(c, \mathcal{P})$ is minimal w.r.t the cost function $g(\varepsilon_c)$, i.e. $\nexists \varepsilon' \in \mathcal{C}(c, \mathcal{R}) : g(\varepsilon') < g(\varepsilon_c)$.*

Proof (Sketch). Algorithm 4 finds alignment ε_c inside the while loop in function align (5-21). Potential alignments are inserted into a queue in lines 19, 17 and 20. In line 10, a candidate alignment is chosen from the queue with a minimal cost function value with respect to ρ . In each iteration of the while loop, the active candidate alignment is checked for being final in line 12. Once a candidate alignment ε_c is found final, it is returned by the function. Since all candidate alignments ε in the queue are selected and then removed according to their cost function value $\rho(\varepsilon)$ in increasing

order, the first alignment that is a proper alignment for trace c will have a minimal value for $\rho(\varepsilon_c)$. If $h(x) = 0$ would hold, then the candidate alignment would always be picked according to the cost function g and trivially the first final alignment would also be optimal, since all alignments with smaller costs had been investigated. \square

Observe that for all final states $f \in R_{\mathcal{P}}$, $h(f) = 0$, since every final state in the PSP represents a proper alignment and a proper alignment fully represents the trace, i.e. $F_{Log} = \emptyset$, and its projection on the reachability graph represents a path, i.e. $F_{Model} = \emptyset$. It follows that ε_c is optimal w.r.t. ρ , when function h underestimates the cost to the optimal cost for any investigated node, which is in line with the optimality criterion of the A^* -search algorithm [28].

We show that our definition of function h fulfils this criterion by analyzing how it estimates future hides for any given node. Let node x be a candidate node, function h compares the multiset of future log labels, determined by trace c set minus the already aligned trace labels $\varepsilon(x)|_{\mathcal{P}}$, with every possible multiset of future model labels to all possible final markings. The multisets of future task labels represent possible paths in the reachability graph to a final marking and a path to a final node in the DAFSA representing the suffix of trace c . By comparing multisets to find deviations, the context of task labels is dropped and h allows for a lower cost than g . Repeated task labels are also assumed to be matched in these multisets and thus are not taken into account in the comparison. Finally, function h minimizes the difference of all multiset comparisons such that it always finds the closest final marking in terms of distance. Given that the multisets represent possible paths, the value of h can only be as high as the true cost of a path and will underestimate the cost in case the abstractions obscure differences due to context or cyclic structures. Thus, h underestimates the true cost to the closest final marking and thus the alignment ε_c is minimal with respect to ρ .

5. Taming concurrency with S-Components

The automata-based technique presented in the previous section suffers from a fundamental scalability limitation due to the fact that it needs to materialize the reachability graph and the size of the reachability graph increases exponentially with the number of parallel activities. This section presents a novel (quasi-optimal) divide-and-conquer approach based on the decomposition of the model into parallelism-free sub-models, so called S-Components. Figure 10 outlines the proposed approach consisting on the following steps: (1) divide the model into S-Components, (2) derive sub logs via trace projection, (3) compute the reachability graphs of the S-Components, (4) compress each sub-log into a DAFSA, (5) compute the sub-PSPs for the reachability graphs (see Step 3) and the corresponding DAFSAs, and (6) recompose the related results to find quasi-optimal alignments.

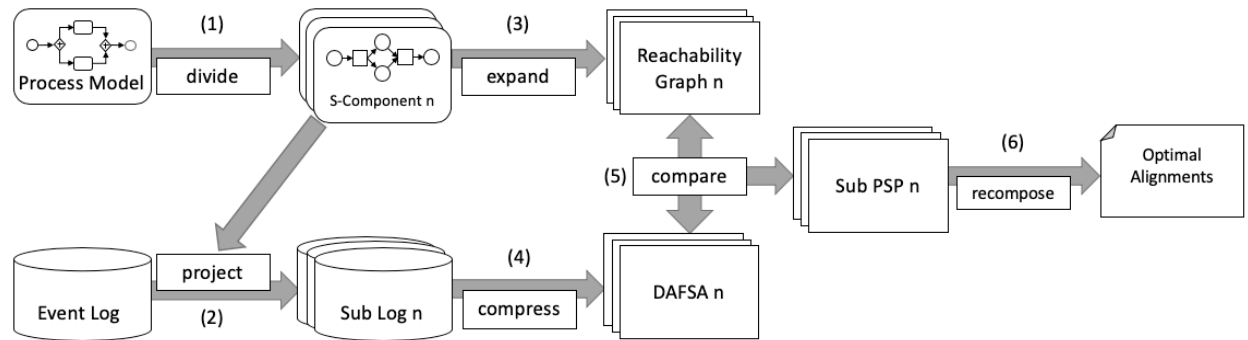


Figure 10. Overview of the S-Component approach.

5.1. Decomposition of the Petri net

The decomposition approach considers uniquely-labelled sound free-choice workflow nets, a subclass of workflow nets [21, 29]. A workflow net is uniquely labelled if every non-silent label is assigned to at most one transition. Soundness was defined in Sect. 3.2. A net is *free-choice* iff whenever two transitions t_1 and t_2 share a common pre-place s , then s is their only pre-place; in a free-choice net concurrency and choices are clearly separated. The formal definitions are given below.

Definition 5.1 (Uniquely-labelled sound free-choice workflow net). *A labelled workflow net $WN = ((P, T, F, \lambda), i, o)$ is free-choice iff for any two transitions $t_1, t_2 \in T$: $s \in \bullet t_1 \cap \bullet t_2$ implies $\bullet t_1 = \bullet t_2 = \{s\}$. A workflow net is uniquely-labelled, iff for any $t_1, t_2 \in T_N$, $\lambda(t_1) = \lambda(t_2) \neq \tau \implies t_1 = t_2$. A system net is uniquely-labelled, sound, and free-choice if the underlying workflow net is.*

An S-Component [21, 29] of a net is a substructure, where every transition has one incoming and one outgoing arc (it does not contain parallelism). A well-formed free-choice workflow net is covered by S-Components and every place, arc and transition of the workflow net is contained in at least one S-Component, which is also a workflow net. Figure 12 shows 4 different S-components of the running example of Fig. 2. Each S-Component contains one of the four tasks A, B, C or D that can be executed in parallel. Note that S-component overlap on non-concurrent parts of the net, e.g., on p_9 , as indicated by nodes with solid borders.

Before we explain the decomposition of a workflow net into S-Components, we need to introduce the concept of the incidence matrix of a Petri-net. Recall from Sect. 3.2 that a marking $m = \langle m(p_1), \dots, m(p_k) \rangle^T$ is a column vector over the places $P = \{p_1, \dots, p_k\}$; and vectors $N^-(t)$ and $N^+(t)$ describe the tokens consumed and produced by t on each $p \in P$. The resulting *effect* of t on P is $N(t) = N^-(t) + N^+(t)$. The *incidence matrix* of a net N is the matrix $N = \langle N(t_1) \dots N(t_r) \rangle$ of the effects of all transitions $T = \{t_1, \dots, t_r\}$. Given a firing sequence σ in WN starting in m_0 , let the row vector $y = \langle y_1, \dots, y_r \rangle$ specify how often each $t_i, i = 1, \dots, r$ occurred in σ . For any such row vector, the *marking equation* $m = m_0 + N \cdot y$ yields the marking reached by firing σ . Figure 11 shows how the marking equation of the Petri net of our sample loan application process in Fig. 2 gives a new marking from the initial marking.

$$\begin{array}{c} \vec{m}_0 \\ \text{start} \\ p_1 \\ p_2 \\ p_3 \\ p_4 \\ p_5 \\ p_6 \\ p_7 \\ p_8 \\ p_9 \\ p_{10} \\ p_{11} \\ p_{12} \\ \text{end} \end{array} \begin{pmatrix} 1 \\ 0 \\ 0 \\ 0 \\ 0 \\ 0 \\ 0 \\ 0 \\ 0 \\ 0 \\ 0 \\ 0 \\ 0 \\ 0 \end{pmatrix} + \begin{pmatrix} \tau & A & B & C & D & \tau & E & F & G & H & I & \tau \\ -1 & 0 & 0 & 0 & 0 & 0 & 0 & 0 & 0 & 0 & 0 & 0 \\ 1 & -1 & 0 & 0 & 0 & 0 & 0 & 0 & 0 & 0 & 0 & 0 \\ 1 & 0 & -1 & 0 & 0 & 0 & 0 & 0 & 0 & 0 & 0 & 0 \\ 1 & 0 & 0 & -1 & 0 & 0 & 0 & 0 & 0 & 0 & 0 & 0 \\ 1 & 0 & 0 & 0 & -1 & 0 & 0 & 0 & 0 & 0 & 0 & 0 \\ 0 & 1 & 0 & 0 & 0 & -1 & 0 & 0 & 0 & 0 & 0 & 0 \\ 0 & 0 & 1 & 0 & 0 & -1 & 0 & 0 & 0 & 0 & 0 & 0 \\ 0 & 0 & 0 & 1 & 0 & -1 & 0 & 0 & 0 & 0 & 0 & 0 \\ 0 & 0 & 0 & 0 & 1 & -1 & 0 & 0 & 0 & 0 & 0 & 0 \\ 0 & 0 & 0 & 0 & 0 & 1 & -1 & 0 & 0 & 1 & 0 & 0 \\ 0 & 0 & 0 & 0 & 0 & 0 & 1 & -1 & -1 & 0 & 0 & 0 \\ 0 & 0 & 0 & 0 & 0 & 0 & 0 & 0 & 1 & -1 & 0 & 0 \\ 0 & 0 & 0 & 0 & 0 & 0 & 0 & 1 & 0 & 0 & -1 & -1 \end{pmatrix} * \begin{pmatrix} \tau & A & B & C & D & \tau & E & F & G & H & I & \tau \\ 1 & 1 & 1 & 1 & 1 & 1 & 2 & 0 & 1 & 1 & 1 & 0 \end{pmatrix} = \begin{array}{c} \vec{m} \\ \text{start} \\ p_1 \\ p_2 \\ p_3 \\ p_4 \\ p_5 \\ p_6 \\ p_7 \\ p_8 \\ p_9 \\ p_{10} \\ p_{11} \\ p_{12} \\ \text{end} \end{array} \begin{pmatrix} 0 \\ 0 \\ 0 \\ 0 \\ 0 \\ 0 \\ 0 \\ 0 \\ 0 \\ 0 \\ 1 \\ 0 \\ 0 \\ 0 \end{pmatrix}$$

Figure 11. Marking equation to reach marking (p_{10}) for our loan application example.

The decomposition of a sound free-choice Petri net into S-Components is based on its place invariants. A *place invariant* is an integer solution J to the equation $J \cdot N = 0$ describing that the number of tokens (weighted by J) is constant over all reachable markings, i.e., $J \cdot m_0 = J \cdot m$ for all reachable markings m of N , because $J \cdot N \cdot y = 0$ [29]. The equation $J \cdot N = 0$ has an infinite number of solutions. We are interested the unique set of *PI non-trivial* place invariants (different from 0) that are *minimal* (not linear combinations of other place invariants of N) can be obtained through standard linear-algebra techniques. Each minimal place invariant J possibly defines an S-Component as a subnet of the workflow net consisting of the *support* $\langle J \rangle$ of J [29]. The workflow net can be decomposed into n S-Component subnets, where n is the number of minimal place invariants of the workflow net, i.e. $|PI|$. We next define a S-Component net and the decomposition of a workflow net.

Definition 5.2 (S-Component, S-Component decomposition). *Let $WN = ((P_N, T_N, F_N, \lambda_N), i, o)$ be a sound, free-choice workflow net. Let J be a minimal place invariant of WN . An S-Component WN_J is a non-empty, strongly connected labelled workflow net $WN_J = ((P_J, T_J, F_J, \lambda_J), i, o)$ with the following properties:*

- $P_J = \{p \in P_N \mid p \in \langle J \rangle \wedge \bullet p \subseteq T_J \wedge p \bullet \subseteq T_J\}$
- $T_J = \{t \in T_N \mid |\bullet t \cup P_J| = 1 = |t \bullet \cup P_J|\}$

- $F_J = \{(p, t) \in F_N \mid p \in P_J \wedge t \in T_J\} \cup \{(t, p) \in F_N \mid t \in T_J \wedge p \in P_J\}$
- $\lambda_J = \{(t, l) \in \lambda_N \mid t \in T_J\}$

For the set of all minimal place invariants PI of WN , the S-Component decomposition \mathcal{C} is a non-empty set of S-Component workflow nets that cover WN , i.e. $\mathcal{C} = \{WN_J \mid J \in PI\}$.

S-Components are concurrency-free, as the requirement $|\bullet t \cup P_J| = 1 = |t \bullet \cup P_J|$ allows only one input / output place per transition. Applying the decomposition to our running example, four minimal place invariants are computed: $(1\ 1\ 0\ 0\ 0\ 1\ 0\ 0\ 0\ 1\ 1\ 1\ 1\ 1)$, $(1\ 0\ 1\ 0\ 0\ 0\ 1\ 0\ 0\ 1\ 1\ 1\ 1\ 1)$, $(1\ 0\ 0\ 1\ 0\ 0\ 0\ 1\ 0\ 1\ 1\ 1\ 1\ 1)$ and $(1\ 0\ 0\ 0\ 1\ 0\ 0\ 0\ 1\ 1\ 1\ 1\ 1)$. Figure 12 shows the derived four S-Component workflow nets; each S-Component contains one of the four tasks A , B , C or D that can be executed in parallel.

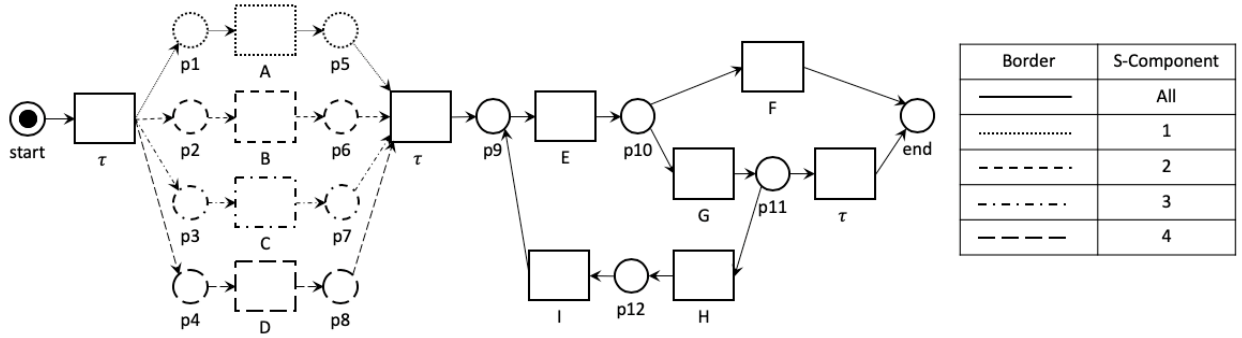


Figure 12. S-Component decomposition of the example loan application process model.

5.2. Conformance checking with S-Component decomposition

This section introduces a novel divide-and-conquer approach to speed up the conformance checking between a system net and an event log. The division of the problem relies on the decomposition of the workflow net into S-Component workflow nets as introduced in Section 5.1.

The following definition introduces *trace projection*, an operation that filters out the events with labels not contained in the alphabet of a particular S-Component.

Definition 5.3 (Trace Projection). A trace projection, denoted as $\upharpoonright_{\lambda}$, is an operation over a trace $c = \langle l_1, l_2, \dots, l_n \rangle$ that filters out all the labels not contained in λ , i.e. $c \upharpoonright_{\{l_i, l_j, \dots, l_k\}} = \langle l_i, l_j, \dots, l_k \rangle$ such that $0 \leq i \leq j \leq \dots \leq k \leq n$.

The novel divide-and-conquer approach decomposes the workflow nets into concurrency-free sub-workflow nets – S-Components –, computing partial alignments between projected traces and S-components, and recomposing the partial alignments to create alignments for each trace in the log. Note that the alignments are partial because the projected traces are only parts of a complete trace. In the following, we explain the full procedure, illustrated in Fig. 13 and defined in Alg. 5, as we obtain and re-compose partial alignments for the trace $\langle B, D, A, E, F, G \rangle$ in our running example and the S-Component workflow nets (Fig. 12). Observe that in our running example there are four S-Component workflow nets, each representing the execution of one of the parallel activities A, B, C and D .

Algorithmic idea. Algorithm 5 starts by computing the reachability graphs for each of the computed S-Components SN_i (having alphabet L_i), as well as the DAFSAs of the projected logs with alphabet L_i (see Lines 1-3). It continues by taking each trace in the log, in this case the trace $\langle B, D, A, E, F, G \rangle$, and projecting it onto the alphabet of each S-component $c \upharpoonright_{L_i}$. Thus, four partial traces are created: $\langle B, E, F, G \rangle$, $\langle D, E, F, G \rangle$, $\langle E, F, G \rangle$ and $\langle A, E, F, G \rangle$. The traces share the subsequence $\langle E, F, G \rangle$ as the corresponding transitions are in the sequential part of the net and hence in all S-components in Fig. 12.

Then, we compute the deterministic optimal alignment ε_i of each projected trace $c \upharpoonright_{L_i}$ to its S-component SN_i (by calling Alg. 4 in line 5 of Alg. 5); we call each ε_i a *projected alignment*. Figure 13 shows the four optimal alignments ε_1 - ε_4 retrieved by Alg. 4 for our running example. Note that because each SN_i is sequential, the reachability graph of

each SN_i has the same size as SN_i itself. Thus the k projected alignment problems are exponentially smaller than the alignment problem on the reachability graph of the original SN .

Once the partial alignments have been computed, we iterate over the original trace c and *compose* the projected alignments $\varepsilon_i = \langle \beta_1^i \beta_2^i \dots \beta_{n_i}^i \rangle$ between \mathcal{D}_i and \mathcal{R}_i of SN_i , $i = 1, \dots, k$ along all “shared” synchronizations into a “global” composed alignment ε_c between \mathcal{D} and \mathcal{R} of SN . For example, in Fig. 13, all projected alignments have a “shared” synchronization *match*(E) (as E is shared by all 4 S-components), so we first advance in each ε_1 – ε_4 over their non-shared synchronizations (one step in each individual S-component) and then compose all *match*(E) synchronizations of ε_1 – ε_4 into one *match*(E) synchronization of ε_c .

Technically, we compose the projected alignments ε_i into ε_c by composing the arcs of all the \mathcal{D}_i and of all the \mathcal{R}_i along the trace c . The composed arcs over the \mathcal{D}_i have to form a path through \mathcal{D} and the composed arcs over the \mathcal{R}_i have to form a path through \mathcal{R} . Then ε_c is an alignment of c to SN by Def. 4.4.

Partially composing k FSMs. Recall that each synchronization $\beta^i = (op_i, b_i, a_i)$ of a projected alignment ε_i refers to an arc $b_i = (n_i, \ell, n'_i)$ of DAFSA \mathcal{D}_i and/or an arc $a_i = (m_i, \ell, m'_i)$ of the reachability graph \mathcal{R}_i of SN_i ; \mathcal{D}_i and \mathcal{R}_i are FSMs.

Next we describe how we technically compose nodes and arcs of $\mathcal{D}_i, i = 1, \dots, k$ and $\mathcal{R}_i, i = 1, \dots, k$, respectively, into composed nodes (as vectors of nodes) and composed arcs (as partial vectors of arcs). The data structures resemble those of the PSP in Def. 4.6. A *composed node* of all the $\mathcal{R}_i, i = 1, \dots, k$ is vector $\underline{m} = \langle m_1, \dots, m_k \rangle, m_i \in N_{\mathcal{R}_i}$; and, $\underline{n} = \langle n_1, \dots, n_k \rangle, n_i \in N_{\mathcal{D}_i}$ is a composed node of all the \mathcal{D}_i .

We will compose nodes and arcs of $\mathcal{D}_i, i = 1, \dots, k$ and $\mathcal{R}_i, i = 1, \dots, k$ along the visible events in the trace c . The composition begins at the initial composed nodes $\underline{n} = \langle s_{\mathcal{D}_1}, \dots, s_{\mathcal{D}_k} \rangle$ and $\underline{m} = \langle s_{\mathcal{R}_1}, \dots, s_{\mathcal{R}_k} \rangle$ (lines 7-8 of Alg. 5). We iterate over the trace c with a counter pos_c and advance separate counters $pos_i, i = 1, \dots, k$ for each component (line 9-10 of Alg. 5). The “next” synchronization $\beta_{pos_i}^i, i = 1, \dots, k$ in each partial alignment gives an arc a_i of \mathcal{R}_i and/or an arc b_i of \mathcal{D}_i . We *partially* compose a subset of those arcs sharing the same label (lines 11-39) as explained next.

First, we give some technical notation for partially composing the \mathcal{D}_i and \mathcal{R}_i arcs, and then we explain the loop for the composition.

Suppose we are at the composed marking $\underline{m} = \langle m_1, \dots, m_k \rangle$ of all the \mathcal{R}_i , and the next arcs we shall follow in the \mathcal{R}_i are $a_1, \dots, a_k, a_i = (m_i, \ell, m'_i)$. We may follow only those arcs *together* that share the same label. The *partial composition* of these arcs for some label ℓ is the vector $\underline{a} = \langle \hat{a}_1, \dots, \hat{a}_k \rangle$ with $\hat{a}_i = a_i$ if $\ell(a_i) = \ell$ and $\hat{a}_i = \perp$ otherwise. For any component i where $\hat{a}_i \neq \perp$, the state changes from m_i to m'_i and all other components remain in their state. Technically, we write $m_i \blacktriangleright (m_i, \ell, m'_i) = m'_i$ and $m_i \blacktriangleright \perp = m_i$ which we lift to $\underline{m} \blacktriangleright \underline{a} = (m_1 \blacktriangleright \hat{a}_1, \dots, m_k \blacktriangleright \hat{a}_k)$. Thus, \underline{a} traverses all those arcs with label ℓ and $\underline{m} \blacktriangleright \underline{a}$ is the composed successor marking reached by this partial synchronization. These definitions equally apply for composing arcs of the \mathcal{D}_i .

Partially composing alignments. We now can explain how we compose the projected alignments ε_i into ε_c by composing the arcs of the \mathcal{D}_i and \mathcal{R}_i in the order in which they occur in the $\varepsilon_i, i = 1, \dots, k$. We “replay” trace c starting from an empty composed alignment, all projected alignments are at $pos_i = 0$, and at the initial composed nodes \underline{n} and \underline{m} for the \mathcal{D}_i and \mathcal{R}_i .

The next event to replay is $\ell = c(pos_c)$ (line 11 of Alg. 5). The next projected synchronizations are $\beta_i = \varepsilon_i(pos_i), i = 1, \dots, k$ with $\beta_i = (op_i, a_i, b_i)$. Two cases may arise.

1. For all S-components i that have $\ell \in L_i$ in their alphabet, their next synchronization β_i involves arcs labeled with $\ell = \ell(\beta_i)$; lines (25-39 in Alg. 5). In this case, all S-components “agree” and we can synchronize the \mathcal{D}_i arcs and the \mathcal{R}_i arcs in the β_i of those S-components into a synchronization for ℓ in ε_c . Again, three cases may arise.
 - (a) All synchronizations β_i labeled with ℓ agree on the operation *lhide* (lines 25-29 in Alg. 5). The partially composed arc $\underline{a}' = (\underline{n}, \ell, \underline{n} \blacktriangleright \underline{a})$ of the \mathcal{D}_i in the new synchronization (*lhide*, \underline{a}', \perp) describes that all S-components make a *lhide* step together (i.e., no S-component fires a transition for event ℓ). The new synchronization is appended to ε_c and we advance the position pos_i for all S-components involved in this composition.
 - (b) All synchronizations β_i labeled with ℓ agree on the operation *match* (lines 30-36 in Alg. 5). We append to ε_c a new *match* synchronization with partially composed \mathcal{D}_i arcs and \mathcal{R}_i arcs, describing that all involved S-components make a *match* step together.

- (c) The partial alignments of some S-components disagree on the operation, i.e., we have conflicting partial solutions (lines 37-39). In this case we fall back to computing a global alignment without decomposition (line 40).
2. There are S-components i that have $\ell \in L_i$ in their alphabet, but the next synchronization β_i is not labeled with $\ell \neq \ell(\beta_i)$ (the set \mathcal{C}_i in line 12 of Alg. 5). These S-components have to “catch up” with *rhide* synchronizations to reach a state where they can participate in a *lhide* or *match* synchronization over ℓ (lines 13-24). However, such S-components may only catch up together: Suppose there is an S-component i having as next synchronization an *rhide* over $\ell(\beta_i) = x \neq \ell$, then *all* S-components with x in their alphabet (set lab_x in line 15) must have an *rhide* synchronization on x as their next synchronization (set $sync_x$ in line 14). If we find such a set (line 16), then we can compose a *rhide* synchronization from the \mathcal{R}_i arcs in $sync_x$ and append it to ε_c . This step may have to be repeated if there is another S-component that still has to catch up. If the projected alignments disagree on the next *rhide*, we have conflicting partial solutions and fall back to computing a global alignment without decomposition (lines 22-24).

Note that in this way, we consecutively construct two paths: one through the composition of the \mathcal{D}_i (by the $\underline{a}' = (\underline{n}, \ell, \underline{n} \triangleright \underline{a})$ arcs) and one through the composition of the \mathcal{R}_i . In Sect. 5.4 we formally state that these paths correspond to paths through \mathcal{D} and \mathcal{R} and thus ε_c is an alignment; the proof is given in Appendix C.

Explanation by example. In the example of Fig. 13, the partial alignments ε_1 - ε_4 are composed to ε_c as follows. For the first event B of c , all S-components involving B (which is the single S-component 2 in this case) agree on a match synchronization $m(B)$ (line 30 of Alg. 5). The composed $m(B)$ synchronization (involving only the \mathcal{D}_2 and \mathcal{R}_2 arcs of S-component 2) are added to ε_c . Note that this corresponds to reaching the marking $[p6]$ in S-component 2 in Fig. 12 while S-components 1, 3, and 4 remain in $[p1]$, $[p3]$, and $[p4]$, respectively. Similarly, for the next events D and A of c , $m(D)$ and $m(A)$ synchronizations are added, which corresponds to reaching $[p8]$ and $[p5]$ in S-components 1 and 4.

The fourth event E occurs in all S-components, but S-component 3 has no E -synchronization yet (line 13 of Alg. 5). In Fig. 12, this corresponds to S-component 3 still being in marking $[p3]$ and transition E not being enabled yet. Instead, ε_3 has an *rhide* synchronization for C . The composed $r(C)$ synchronization involves only \mathcal{R}_3 arcs of S-component 3. Now all S-components agree on $m(E)$ synchronizations (the common τ -transition in Fig. 12 was removed from all reachability graphs), thus $m(E)$ is added to ε_c in step 4.2; in the synchronization arcs from all \mathcal{D}_i and all \mathcal{R}_i are involved as in each S-component 1-4, the marking $[p10]$ is reached. The algorithm proceeds similarly in steps 5 and 6 by adding a *match* synchronization for label F and a *lhide* synchronization for label G since all projected alignments agree on those synchronizations. The resulting sequence ε_c of synchronizations is a proper alignment according to Def. 4.4.

Step	1	2	3	4.1	4.2	5	6
c	B	D	A	E		F	G
ε_1	m(A)			m(E)		m(F)	l(G)
ε_2	m(B)	m(E)			m(F)	l(G)	
ε_3	r(C)			m(E)	m(F)	l(G)	
ε_4	m(D)		m(E)		m(F)	l(G)	
ε_c	m(B)	m(D)	m(A)	r(C)	m(E)	m(F)	l(G)

Figure 13. Example for applying Alg. 5 to trace $\langle B, D, A, E, F, G \rangle$ to our running example.

5.3. Optimality is not guaranteed under recomposition

The recomposition of partial alignments in Alg. 5 is not necessarily optimal. Figure 14 shows a pair of S-Components, each representing a parallel activity A or B followed by a merging activity C and a trace $\langle C, A, B \rangle$,

Algorithm 5: Construct PSP by Recomposing S-Component Alignments

input: Event Log \mathcal{L} , DAFSA \mathcal{D} , System net $SN = (WN, m_0, M_f)$ with its S-Component decomposition $\mathcal{C} = \{WN_1, \dots, WN_k\}$;

- 1 $\mathcal{R}_i \leftarrow$ reachability graph of $SN_i = (WN_i, m_0, M_f)$ for each $i = 1, \dots, k$;
- 2 $L_i \leftarrow$ labels occurring in WN_i for each $i = 1, \dots, k$;
- 3 $\mathcal{D}_i \leftarrow$ construct DAFSA($\{c|_{L_i} \mid c \in \mathcal{L}\}$) for each $i = 1, \dots, k$;
- 4 **for** Trace $c \in \mathcal{L}$ **do**
- 5 $\varepsilon_i \leftarrow \text{align}(c|_{L_i}, \mathcal{D}_i, \mathcal{R}_i)$ with Alg. 4 for each $i = 1, \dots, k$;
- 6 $\varepsilon_c \leftarrow \langle \rangle$;
- 7 $\underline{n} \leftarrow (n_{\mathcal{D}}(\varepsilon_1(0)), \dots, n_{\mathcal{D}}(\varepsilon_k(0)))$;
- 8 $\underline{m} \leftarrow (m_{\mathcal{D}}(\varepsilon_1(0)), \dots, m_{\mathcal{D}}(\varepsilon_k(0)))$;
- 9 $pos_i \leftarrow 0$ for each $i = 1, \dots, k$;
- 10 **for** $pos_c \leftarrow 1 : |c| + 1$ **do**
- 11 $\ell \leftarrow c[pos_c]$;
- 12 $\mathcal{C}_\ell \leftarrow \{(i, \varepsilon_i) \mid i = 1 \dots k \wedge pos_i \leq |\varepsilon_i| \wedge ((\ell \in L_i \wedge \ell(\varepsilon_i(pos_i)) \neq \ell) \vee (\ell = \perp))\}$;
- 13 **while** $\mathcal{C}_\ell \neq \emptyset$ **do**
- 14 $sync_x \leftarrow \{(i, \varepsilon_i) \mid \ell(\varepsilon_i(pos_i)) = x \wedge op(\varepsilon_i(pos_i)) = rhide\}$ for each label $x \in L$;
- 15 $lab_x \leftarrow \{(i, \varepsilon_i) \mid x \in L_i\}$ for each label $x \in L$;
- 16 **if** $\exists x \in L : sync_x = lab_x$ **then**
- 17 $a_i \leftarrow \begin{cases} \varepsilon_i(pos_i)^{a_{\mathcal{D}}} & \text{if } (i, \varepsilon_i) \in sync_x \\ \perp & \text{otherwise} \end{cases}$, for each $i = 1, \dots, k$;
- 18 $\varepsilon_c \leftarrow \varepsilon_c \oplus (rhide, \perp, (\underline{m}, x, \underline{m} \blacktriangleright (a_1, \dots, a_k)))$;
- 19 $\underline{m} \leftarrow \underline{m} \blacktriangleright (a_1, \dots, a_k)$;
- 20 $pos_i \leftarrow pos_i + 1$ for each $(i, \varepsilon_i) \in sync_x$;
- 21 $\mathcal{C}_\ell \leftarrow \{(i, \varepsilon_i) \mid i = 1 \dots k \wedge pos_i \leq |\varepsilon_i| \wedge ((\ell \in L_i \wedge \ell(\varepsilon_i(pos_i)) \neq \ell) \vee (\ell = \perp))\}$;
- 22 **else**
- 23 assert label conflict($\varepsilon_c, \ell, rhide$);
- 24 jump to line 40;
- 25 **if** $(\forall i = 1 \dots k \mid \ell \in L_i \implies op(\varepsilon_i(pos_i)) = lhide) \wedge \ell \neq \perp$ **then**
- 26 $b_i \leftarrow \begin{cases} \varepsilon_i(pos_i)^{a_{\mathcal{D}}} & \text{if } \ell \in L_i \\ \perp & \text{otherwise} \end{cases}$, for each $i = 1, \dots, k$;
- 27 $\varepsilon_c \leftarrow \varepsilon_c \oplus (lhide, (\underline{n}, \ell, \underline{n} \blacktriangleright (b_1, \dots, b_k)), \perp)$;
- 28 $\underline{n} \leftarrow \underline{n} \blacktriangleright (b_1, \dots, b_k)$;
- 29 $pos_i \leftarrow pos_i + 1$ for each $i = 1, \dots, k$ where $\ell \in L_i$;
- 30 **else if** $(\forall i = 1 \dots k \mid \ell \in L_i \implies op(\varepsilon_i(pos_i)) = match) \wedge \ell \neq \perp$ **then**
- 31 $b_i \leftarrow \begin{cases} \varepsilon_i(pos_i)^{a_{\mathcal{D}}} & \text{if } \ell \in L_i \\ \perp & \text{otherwise} \end{cases}$, for each $i = 1, \dots, k$;
- 32 $a_i \leftarrow \begin{cases} \varepsilon_i(pos_i)^{a_{\mathcal{D}}} & \text{if } \ell \in L_i \\ \perp & \text{otherwise} \end{cases}$, for each $i = 1, \dots, k$;
- 33 $\varepsilon_c \leftarrow \varepsilon_c \oplus (match, (\underline{n}, \ell, \underline{n} \blacktriangleright (b_1, \dots, b_k)), (\underline{m}, \ell, \underline{m} \blacktriangleright (a_1, \dots, a_k)))$;
- 34 $\underline{n} \leftarrow \underline{n} \blacktriangleright (b_1, \dots, b_k)$;
- 35 $\underline{m} \leftarrow \underline{m} \blacktriangleright (a_1, \dots, a_k)$;
- 36 $pos_i \leftarrow pos_i + 1$ for each $i = 1, \dots, k$ where $\ell \in L_i$;
- 37 **else if** $\ell \neq \perp$ **then**
- 38 S-Components disagree \rightarrow assert operation conflict($\varepsilon_c, \ell, lhide$);
- 39 jump to line 40;
- 40 **if** Any conflict occurred **then** $\varepsilon_c \leftarrow \text{align}(c, \mathcal{D}, \mathcal{R})$ with Algorithm 2;
- 41 InsertIntoPSP($\varepsilon_c, c, \mathcal{P}$);
- 42 **return** \mathcal{P} ;

where the merging activity is miss-allocated before the parallel activities. The two optimal projected alignments according to the sorting from subsection 4.4 then each include a *rhide* synchronization for the parallel activity, a *match* synchronization for the merging activity C and a *lhide* synchronization for the parallel activity. Note that both projected alignments are optimal in cost. Once the projected alignments are recomposed, the cost of the recomposed alignment is 4: $\langle r(A), r(B), m(C), l(A), l(B) \rangle$. However, there exists another proper alignment with a lower cost of 2: $\langle l(C), m(A), m(B), r(C) \rangle$. The reason why the recomposed alignment is not optimal, while the projected alignments are optimal, is that the projected alignments choose one optimal alignments out of multiple possible optimal alignments with the same cost without considering which choices would globally minimize the cost when recomposing the projected alignments. In this example, the projected alignments with another kind of sorting could also be $\langle l(C), m(A), r(C) \rangle$ and $\langle l(C), m(B), r(C) \rangle$, which would recompose to the optimal alignment. With the current sorting introduced in subsection 4.4, we introduce an additional cost of one over the optimal cost per S-Component workflow net for a task miss-allocation of a merging activity possibly multiple times, when the parallel block is enclosed in a cyclic structure. Hence, the worst-case cost over-approximation of the proposed recomposition algorithm for a

given trace c is $k * \#i$, where k is the size of the S-Component decomposition and $\#i$ is the number of maximal repetitions of a label in c that is also contained in a parallel block in the process model. Transforming the recomposition procedure into a minimization problem of selecting the best projected alignments for recomposition would however increase the calculation overhead exponentially since every trace can have exponentially many optimal alignments for each S-Component workflow net. Thus, selecting the best optimal projected alignments can be computationally more expensive than calculating only one-optimal alignments for the initial workflow net and event log. However, calculating the reachability graphs of workflow nets without parallel constructs is polynomial in size, speeding up the calculation of one optimal-projected alignments, and thus the proposed technique can provide significant speed-ups over the original technique on process models with parallelism.

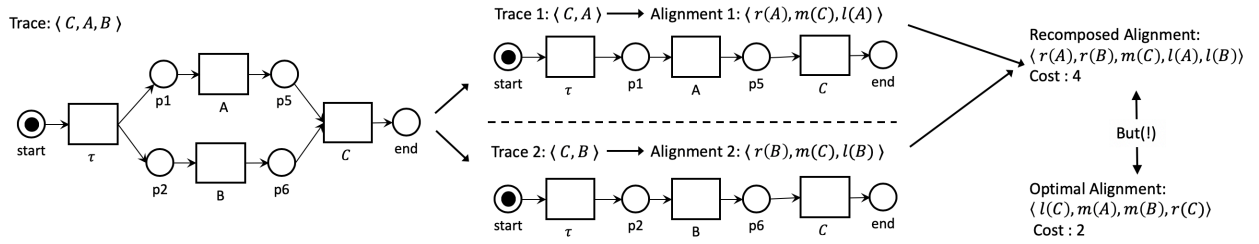


Figure 14. Counter-example to optimality of a recomposed alignment.

Even though the presented approach computes non-optimal results, the evaluation shows that both the fraction of affected traces as well as the degree of over-approximation is rather low. The results obtained for the evaluation of this novel approach is oftentimes close to optimal.

5.4. Addressing invisible label conflicts

The recomposition of synchronizations from the partial alignments of the S-components in Alg. 5 relies on the unique labeling. In this way, arcs in the reachability graphs of different S-components can safely be related to each other. However, if a uniquely labeled process model contains a τ -labeled transition, Alg. 1 reduces these τ -labeled transitions by contraction with subsequent visible edges. This may lead to two arcs in the reachability graph carrying the same label D but describing different effects, a hidden form of label duplication. Applying Alg. 5 on such a model may lead to two partial alignments where the composed synchronization agree on label D , but the underlying arcs in the reachability graphs disagree, leading to a “hidden” recomposition conflict not detected by Alg. 5. The resulting ε_c would no longer form a path through the process model.

In the following, we illustrate the problem by an example and discuss a simple change to Alg. 1 that ensures a unique labeling over all reachability graphs (global and projected). For such reachability graphs, Alg. 5 always returns an alignment, which we prove formally.

Figure 15 shows an example with trace $\langle A, B, D \rangle$ and a process model, where the parallel tasks B and C can be skipped. The process model is decomposed into two S-Component nets, one for each of the two parallel activities. When the trace is projected onto the S-Component with activity C , the obtained alignment matches both trace activities and skips activity C with the τ transition. The sub-trace $\langle A, B, D \rangle$ can be fully matched on the other S-Component. The recomposed alignment is $\langle m(A), m(B), m(D) \rangle$. However, A, B, D is not a path through the reachability graph of this process model.

Note that reducing the reachability graph of the model in Fig. 15 by Alg. 1 leads to two D -labeled arcs: $([p1], D, [end])$ (by the skipping τ -transition) and $([p3, p5], D, [end])$ (by the joining τ -transition). The alignment for the first S-component uses the former whereas the alignment for the second S-component uses the latter, leading to the conflict described above.

Figure 16 illustrates shows how to relabel arcs in the reachability graph to avoid “hidden” label duplication. First, add to each τ -transition a unique index at the start of Alg. 1 so that all τ -transitions are uniquely labeled. Second, we alter Alg. 1 to maintain the identity of the removed τ transitions in the next visible transition. In particular, when replacing an arc (n_1, ℓ, n_2) for an arc with label τ_i , we create an extended label (τ_i, ℓ) for the replacement arc. Let Alg. 1* be this modification of Alg. 1 and let Alg. 5* which invokes Alg. 1* instead of Alg. 1. Alg. 1* and the extended labels are not used for the PSP construction Algs. 2 and 4. We omit the technical details. The changes in Fig. 16 lead

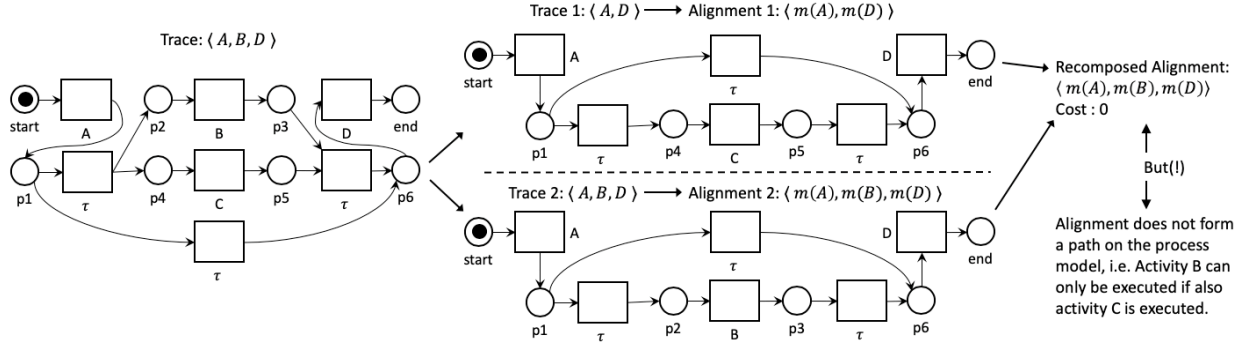


Figure 15. Recomposed alignment that can not be replayed on the process model.

to the following differences: The transition τ_1 can now be distinguished from transition τ_3 . During the recomposition, there will be a label conflict between the extended labels (τ_1, D) and (τ_3, D) . As a result, this trace will be aligned on the original reachability graph to ensure the alignment forms a path through the process model.

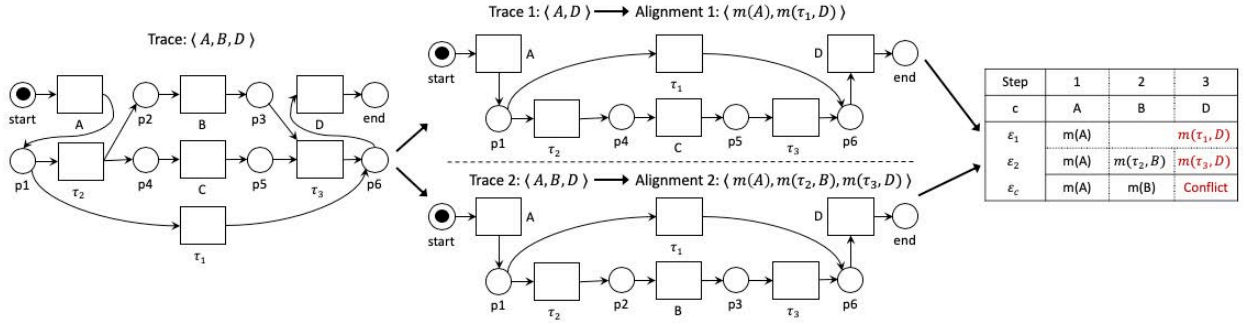


Figure 16. Detecting the invisible label conflict.

The following theorem states that the recomposed alignment is a proper alignment.

Theorem 5.1. Let \mathcal{L} be an event log and $SN = (WN, m_0, m_f)$ be a system net, where WN is a uniquely labeled, sound, free-choice workflow net. Let $\mathcal{P}' = \text{Alg5}^*(\mathcal{L}, \mathcal{D}, SN)$. For every trace $c \in \mathcal{L}$, $\varepsilon_c = \varepsilon(\mathcal{P}', c)$ is a proper alignment. Specifically, the following two properties hold:

1. The sequence of synchronizations with lhide or match operations reflects the trace c , i.e. $\lambda(\varepsilon_c \upharpoonright_{\mathcal{D}}) = c$.
2. The arcs of the reachability graph in the sequence of synchronizations with rhide or match operations forms a path in the reachability graph from the initial to the final marking, i.e. let $n = |\varepsilon_c \upharpoonright_{\mathcal{R}}|$, then $\text{src}(\varepsilon_c \upharpoonright_{\mathcal{R}}[1]) = m_0 \wedge \text{tgt}(\varepsilon_c \upharpoonright_{\mathcal{R}}[n]) = m_f \wedge \forall a_i, a_{i+1} \in \varepsilon \upharpoonright_{\mathcal{R}} \mid 1 \leq i < n : \text{tgt}(a_i) = \text{src}(a_{i+1})$.

The formal proof by induction on the length of c is given in Appendix C. The core argument is to show that the markings and the transition firings of SN can be reconstructed from the vector \underline{m} of markings of each S-component nets. Further, the arcs in the reachability graphs of the S-components nets are isomorphic to the transitions. As a result, the transition effect of the original transition in SN can be recomposed from the effects in the S-component nets. The latter argument requires the uniqueness of arcs in the reachability graphs provided by Alg. 1*.

6. Evaluation

We implemented our approach in a standalone open-source tool.³ Given an event log in XES format and a process model in BPMN or PNML (the latter is the serialization format of Petri nets), the tool will return several conformance

³Tool available at <https://apromore.org/platform/tools>. Source code available at <https://github.com/apromore/DAFSABasedConformance>

statistics such as fitness and raw fitness cost. Optionally, a list of one-optimal alignments for each unique trace as well as their individual alignment statistics can also be extracted. The tool implements both the Automata-based approach described in Section 4 as well as the extended approach with the S-Components improvement described in Section 5.

Using this tool, we conducted a series of experiments to measure the quality and time performance of both our approaches against two state-of-the-art conformance checking techniques: 1) the newest version of the one-optimal alignment with the ILP marking equation, first presented in [30] and implemented in ProM in the PNetReplayer package (ILP Alignments); and 2) the one-optimal alignment approach using the extended marking equation presented in [5] and implemented in ProM in the Alignment package (MEQ Alignments). We implemented multi-threading with each unique trace, and in the S-Components variant, also for each S-Component.

The two benchmark implementations use optimized data structures and efficient hashcodes [31]. Accordingly, we optimized our software implementation using similar techniques, so as to achieve results that are as comparable as possible. Specifically, we optimised the queuing mechanism by improving the selection of suitable solutions, merging overlapping solutions and prioritizing longer solutions with the same cost to faster find an optimal solution.

6.1. Setup

We measured the quality of alignment in terms of alignment cost (Def. 4.7) per trace. We chose to report the alignment cost over other conformance measures such as fitness as it better allows one to pinpoint over-approximation of the result. Given that the complexity of the alignment problem is worst-time exponential, we decided to apply a reasonable time bound of 10 minutes to each experiment. We note that previous experiments reported that in certain cases the computation of an alignment may take over a dozen hours [11]. The experiments were run multi-threaded with a fixed amount of 16 threads for each approach to achieve a comparable computation setup. Each experiment was run five times and we report the average results of runs #2 to #4 to avoid influence of the Java class loader and reduce variance.

The experiments were conducted on a 22-core Intel Xeon CPU E5-2699 v4 with 2.30GHz, with 128GB of RAM running JVM 8. This machine can execute up to 44 threads per socket.

6.2. Datasets

We used two datasets of log-model pairs from a recent benchmark on automated process discovery [32] to investigate the performance of a wide range of different log and process model characteristics. The first dataset consists of twelve public event logs. These logs in turn originate from the 4TU Centre for Research Data⁴. They include the logs of the Business Process Intelligence Challenge (BPIC) series, BPIC12 [33], BPIC13_{cp} [34], BPIC13_{inc} [35], BPIC14 [36], BPIC15 [37], BPIC17 [38], the Road Traffic Fines Management process log (RTFMP) [39] and the SEPSIS Cases log (SEPSIS) [40]. These logs record process executions from different domains such as finance, healthcare, government and IT service management. The BPIC logs from the years 2011 and 2016 were excluded since they do not represent real business processes. We observe that in the benchmark, some of those logs (marked with “*f*”) were filtered from infrequent behavior with the technique in [41] to avoid state-space explosion in the computation of fitness and precision. We retained this filtering step because we experienced the same problem with the unfiltered logs, i.e. it was not possible to compute the raw fitness cost for most of the approaches assessed. Moreover, keeping this filtering allows us to retain exactly the same dataset as used in the benchmark, for compatibility purposes. The second dataset is composed of eight proprietary logs sourced from several organizations around the world, including healthcare, banking, insurance and software vendors.

Each of the two datasets comes with four process models per log, that have been discovered using four state-of-the-art automated discovery methods in the benchmark in [32], namely: Inductive Miner [42], Split Miner [43], Structured Heuristics Miner [44] and Fodina [45]. We discarded the process models discovered by the latter two methods for our experiments since they may lead to process models with transitions with duplicate labels (and in some cases also to unsound models), which our S-Components extension does not handle. This resulted in a total of 40 log-model pairs for our evaluation.

Table 1 reports the log characteristics. We have logs of different sizes in terms of total traces (681–787,667) or total number of events (6,660–1,808,706). The difficulty of the conformance checking problem, however, is more

⁴https://data.4tu.nl/repository/collection:event_logs_real

related to the number of distinct traces (0.01%–97.5%), the number of distinct events (7–82) and the trace length (avg. 1–32). The logs thus feature a wide range of characteristics, from simple to complex logs, for the conformance checking problem. For reference, we made the public logs and corresponding models, together with all the results of our experiments, available online [46].

Log Name	Total Traces	Distinct Traces (%)	Total Events	Distinct Events	Trace Length		
					min	avg	max
BPIC12	13,087	33.4	262,200	36	3	20	175
BPIC13 _{cp}	1,487	12.3	6,660	7	1	4	35
BPIC13 _{inc}	7,554	20.0	65,533	13	1	9	123
BPIC14 _f	41,353	36.1	369,485	9	3	9	167
BPIC15 _{1f}	902	32.7	21,656	70	5	24	50
BPIC15 _{2f}	681	61.7	24,678	82	4	36	63
BPIC15 _{3f}	1,369	60.3	43,786	62	4	32	54
BPIC15 _{4f}	860	52.4	29,403	65	5	34	54
BPIC15 _{5f}	975	45.7	30,030	74	4	31	61
BPIC17 _f	21,861	40.1	714,198	41	11	33	113
RTFMP	150,370	0.2	561,470	11	2	4	20
SEPSIS	1,050	80.6	15,214	16	3	14	185
PRT1	12,720	8.1	75,353	9	2	5	64
PRT2	1,182	97.5	46,282	9	12	39	276
PRT3	1,600	19.9	13,720	15	6	8	9
PRT4	20,000	29.7	166,282	11	6	8	36
PRT6	744	22.4	6,011	9	7	8	21
PRT7	2,000	6.4	16,353	13	8	8	11
PRT9	787,657	0.01	1,808,706	8	1	2	58
PRT10	43,514	0.01	78,864	19	1	1	15

Table 1. Descriptive statistics of the event logs in the public and private datasets

Table 2 reports the statistics of the process models obtained with Inductive (IM) and Split Miner (SM), for each log in our evaluation. Specifically, this table reports size (number of places, transitions and arcs), number of transitions, number gateways (XOR-splits, AND-splits) and size of the resulting reachability graph from the Petri net (in case of a BPMN model, it is the Petri net obtained from this model). In addition, if a Petri net has at least one AND-split, we also report on the number of S-Components and for each of them the following statistics: their average Petri net size, average number of transitions, average number of XOR-splits and average size of the resulting reachability graph.

Inductive Miner is designed to discover highly-fitting models. As a result, the models often exhibit a large reachability graph as the models need to cater for a large variety of executions present in the logs. Split Miner strikes a trade-off between fitness and precision by filtering the directly-follows graph of the log before discovering the model. That leads to process models with a smaller state space, but with a possibly higher number of fitness mismatches. Altogether, these models present two different scenarios for conformance checking: the models discovered by Inductive Miner require a large state space to be traversed with a low to medium number of mismatches per trace, while the models of Split Miner have a smaller state space with a medium to high number of mismatches per trace.

The S-Component decomposition can drastically reduce the size of the state space of the model. This becomes apparent when comparing the size of the reachability graph with that of the S-Component reachability graphs, e.g. BPIC12 (IM) reduces from 1,997 nodes and arcs to a total of 583 nodes and arcs and BPIC14_f from 4,383 to a total of 261 nodes and arcs. This reduction depends on the internal structure of the model, i.e. the number of S-components and the nesting of XOR-splits and AND-splits. Sometimes, this reduction will not lead to a smaller state space, e.g. for BPIC15_{3f} (IM) the size reduces from 875 to 191.5 per S-Component, which leads to a total state space of 1,532 nodes and arcs for all S-Components, which is larger than the size of the original model.

6.3. Results

Table 3 reports the running times in milliseconds (ms) for each approach against each of the 40 log-model pairs, using a fixed number of 16 threads per approach. The best execution time for each experiment is highlighted in bold text.

Miner	Domain	Dataset	Size	Trns	XOR	AND	RG Size	#SComp	Ø Size	Ø Trns	Ø XOR	Ø RG Size
IM	public	BPIC12	177	45	16	2	1,997	10	130.9	36.3	12.3	58.3
		BPIC13 _{cp}	31	8	2	0	9	1	-	-	-	-
		BPIC13 _{inc}	56	13	3	1	121	3	28	7	1	14
		BPIC14 _f	124	29	8	2	4,383	10	53.9	13.9	2.7	26.1
		BPIC15 _{1f}	449	127	48	0	719	1	-	-	-	-
		BPIC15 _{2f}	537	150	55	1	1,019	2	530	149	55	232
		BPIC15 _{3f}	464	128	47	3	875	8	438.5	123.5	45.5	191.5
		BPIC15 _{4f}	469	131	51	1	1,019	2	462	130	51	202
		BPIC15 _{5f}	381	111	31	0	429	1	-	-	-	-
		BPIC17 _f	121	33	8	0	59	1	-	-	-	-
	private	RTFMP	111	26	9	2	2,394	6	52.7	13.8	3.7	25
		SEPSIS	145	37	13	3	2,274	8	99	27.5	9	44
		PRT1	70	16	4	1	195	4	39.3	10	1.8	19.3
		PRT2	175	43	16	1	5,515,357	7	49	13	4	23
		PRT3	111	27	8	2	167	8	71	19	4	33
		PRT4	91	21	5	2	154	8	54	14	2	26
		PRT6	86	20	4	2	65	6	59	15	2	29
		PRT7	99	23	5	2	158	8	62	16	2	30
		PRT9	96	21	7	2	9,121	7	27.9	7	1.1	13.9
		PRT10	124	35	8	1	184	2	115.5	33.5	7.5	48.5
SM	public	BPIC12	315	85	29	1	95	2	308	84	29	140
		BPIC13 _{cp}	49	13	4	0	13	1	-	-	-	-
		BPIC13 _{inc}	56	15	5	0	17	1	-	-	-	-
		BPIC14 _f	88	24	9	0	24	1	-	-	-	-
		BPIC15 _{1f}	368	98	25	0	156	1	-	-	-	-
		BPIC15 _{2f}	444	117	25	0	186	1	-	-	-	-
		BPIC15 _{3f}	296	78	17	0	136	1	-	-	-	-
		BPIC15 _{4f}	323	85	18	0	141	1	-	-	-	-
		BPIC15 _{5f}	359	94	18	0	159	1	-	-	-	-
		BPIC17 _f	149	40	12	0	54	1	-	-	-	-
	private	RTFMP	102	28	11	0	37	1	-	-	-	-
		SEPSIS	162	44	15	0	41	1	-	-	-	-
		PRT1	104	28	9	0	28	1	-	-	-	-
		PRT2	166	45	15	0	37	1	-	-	-	-
		PRT3	96	25	8	1	34	2	89	24	8	41
		PRT4	126	33	10	1	34	2	119	32	10	55
		PRT6	46	11	2	1	20	2	39	10	2	19
		PRT7	86	19	3	5	39	6	57	14.7	2.7	27.7
		PRT9	107	29	10	0	32	1	-	-	-	-
		PRT10	327	90	34	0	92	1	-	-	-	-

Table 2. Descriptive statistics of the process models obtained by IM and SM from the datasets in Table 1

The S-Components approach outperforms the other approaches in 8 out of 40 log-model pairs, the Automata-based technique performs best in 28 out of 40 cases and the extended MEQ Alignments approach outperforms in 3 out of 40 cases. In total, the S-Components approach times out (“t/out” in the table) in 2 cases, the Automata-based approach in 3, ILP Alignments on 1 and the extended MEQ alignments approach times out in 6 cases. All approaches timed out on PRT2 (IM), which has a huge state space of 5,515,357 nodes and arcs in the reachability graph. The S-Components approach actually manages to compute alignments quickly for this log-model pair since the S-Component reachability graphs are very small, but times out when some traces conflict with each other in the recomposition algorithm and need to be aligned on the original reachability graph, which is much larger. The S-Components approach manages to compute alignments for the BPIC14_f (IM), which was not possible within the 10 minutes timeout for the Automata-based approach.

The Automata-based approach performs better than both state-of-the-art approaches ILP and MEQ Alignments by one-two orders of magnitude. For example, for the BPIC17_f (IM) it takes 680 ms against 20.7 sec of ILP Alignments or for BPIC12 (SM) it takes 4,578 ms vs 188,489 ms of ILP Alignments. When the state space reduction of the S-Components is effective, it shows the potential to improve over other approaches by at least one order of magnitude, e.g. for BPIC12 (IM) it improves from 121,845 ms (Automata-based) to 44,301 ms and for BPIC14_f (IM) from 84,102 ms (ILP) to 7,789 ms. In total the Automata-based approach improves over both baseline approaches by one order of magnitude in ten datasets and the S-Component approach in three datasets. The S-Component extension improves over the automata-based approach by one order of magnitude in five cases. The process models discovered by Split Miner do not feature parallel constructs except the model discovered from the BPIC12 log. Thus, in these logs, the performance of the S-Component extension is the same as that of the automata-based approach. In the BPIC12 (SM) case, the Automata-based technique outperforms the S-Component approach because it exploits the parallel constructs in the model. This is due to the combined state-space of the S-Component reachability graphs being larger than the original size of the reachability graph of the process model. This can already happen for process models with a small amount of parallel behavior in comparison to models with a large amount of other behavior, i.e. the model from the BPIC12 log has one parallel block with two parallel transitions against a total of 85 transitions.

Since the advantages of the S-Components decomposition are limited to a specific type of process models (those with large state spaces due to a high degree of parallelism), we derived an empirical rule to decide when to use the S-Components improvement on top of our Automata-based approach. Accordingly, we apply this improvement if the sum of the reachability graph sizes of all S-Components is smaller than that of the original reachability graph of the process model. We added the execution times for this hybrid approach to Table 3. The hybrid approach manages to outperform all other approaches in 30 out of 40 cases and performs second best in five more cases. We note that the reported execution time of the hybrid approach does not include the time required to decide whether or not to apply the S-Components improvement. If we end up selecting the S-Components, we do not actually need additional time, since the reachability graphs for the S-Component nets are computed anyways as part of the decomposition approach. If we select the base approach, this leads to two cases: the model does not have parallelism or it does. If it does not, we detect this case by checking all transitions of the Petri net, which is a linear operation, so the time is negligible. If the model has parallelism, we need to calculate the reachability graphs for every S-Component net. In practice, this time was always negligible in our experiments, but there can be very large process models for which this operation may be expensive. However, in these cases, it is likely that we would select the S-Component approach anyway.

Table 4 shows the optimal costs for a subset of datasets. In these log-model pairs, the S-Components approach over-approximates the optimal cost of the alignments, i.e. in 6 out of 40 cases. For completeness the full table with optimal costs for all datasets can be found in Appendix A. The difference between the S-Component approach and all other approaches with optimal costs ranges from 0.002 to 0.052 per trace. We further broke down the over-approximation into two columns: the fraction of traces in the log that were affected by an over-approximation, which ranges from 0.2 to 5.2%, and the average fitness-cost that was over-approximated in the affected traces, which ranges from 1 to 2 mismatches more than the optimal number. We observe that the approach never under-approximates and always returns proper alignments. By design, the Automata-based approach always has the same cost as the ILP or the MEQ Alignments and thus is always optimal.

One example of over-approximation can be observed in the SEPSIS dataset (IM) for the trace ⟨CRP, Leucocytes, LacticAcid, ER Registration, ER Triage, ER Sepsis Triage, IV Antibiotics, IV Liquid⟩. The optimal alignment for this trace, retrieved with ILP-Alignments, is ⟨(rhide,ER Registration), (match,CRP), (match,Leucocytes), (match,LacticAcid), (lhide,ER Registration), (match,ER Triage), (match,ER Sepsis Triage), (match,IV Antibiotics), (match,IV

Miner	Domain	Dataset	Baselines		Our Approaches		
			ILP Alignments	extended MEQ Alignments	Automata-based Approach	S-Component Approach	Hybrid Approach
IM	public	BPIC12	129,268	464,849	121,845	44,301	44,301
		BPIC13 _{cp}	97	1,362	45	52	45
		BPIC13 _{inc}	1,514	17,857	4,733	155	155
		BPIC14 _f	84,102	143,006	t/out	7,789	7,789
		BPIC15 _{1f}	3,323	1,312	t/out	t/out	t/out
		BPIC15 _{2f}	19,663	4,300	2,423	9,541	9,541
		BPIC15 _{3f}	30,690	15,644	2,042	22,191	2,042
		BPIC15 _{4f}	11,696	6,574	1,023	4,915	4,915
		BPIC15 _{5f}	6,830	2,859	30,648	17,577	30,648
		BPIC17 _f	20,745	63,335	680	3,530	680
	private	RTFMP	1,846	108,818	334	507	507
		SEPSIS	6,592	4,347	31,113	1,575	1,575
		PRT1	868	8,860	774	170	170
		PRT2	t/out	t/out	t/out	t/out	t/out
		PRT3	203	1,176	60	106	60
		PRT4	4,041	14,396	1,021	1,329	1,021
		PRT6	131	582	32	72	32
		PRT7	106	1,456	34	70	34
SM	public	PRT9	30,772	t/out	12,686	4,505	4,505
		PRT10	562	33,813	63	166	166
		BPIC12	188,489	487,878	4,578	68,246	4,578
		BPIC13 _{cp}	128	1,934	28	42	28
		BPIC13 _{inc}	1,120	23,497	140	290	140
		BPIC14 _f	37,987	t/out	3,185	7,792	3,185
		BPIC15 _{1f}	2,972	847	1,528	1,397	1,528
		BPIC15 _{2f}	9,128	1,352	1,036	1,026	1,026
		BPIC15 _{3f}	7,282	2,911	609	934	609
		BPIC15 _{4f}	7,258	1,804	585	655	585
	private	BPIC15 _{5f}	8,805	1,423	765	660	765
		BPIC17 _f	27,011	22,572	727	3,669	727
		RTFMP	1,836	112,328	110	345	110
		SEPSIS	4,912	t/out	276	343	276
		PRT1	1,954	21,642	135	379	135
		PRT2	37,556	t/out	3,830	3,836	3,830
		PRT3	181	1,524	55	89	55
		PRT4	7,433	49,980	475	1,794	475
PRT6		75	603	33	52	33	
PRT7		96	1,439	26	103	26	
Total outperforming:			0	3	28	8	30
			5	3	5	26	5
#Timeouts:			1	6	3	2	2

Table 3. Time performance in milliseconds

Liquid)) with a cost of 2, because task ER Registration is misplaced after the parallel block. The S-Components approach finds instead the following alignment: $\langle (hide, CRP), (hide, Leucocytes), (hide, LacticAcid), (match, ER Registration), (match, ER Triage), (match, ER Sepsis Triage), (match, IV Antibiotics), (match, IV Liquid) \rangle$ with a cost of 3. As shown in Figure 17, in the process model, task ER Registration appears before the parallel block, while in the trace this occurs after the activities in a parallel block. As a result, the S-Component approach will hide all the activities in the parallel block, i.e. CRP, Leucocytes and LacticAcid, and then match the activity ER Registration. When recomposing the projected alignments, however, the added alignment cost will be 3 instead of 2. Note that the alignment of the S-Components approach is still a proper alignment, i.e. still represents the trace and forms a path through the process model.

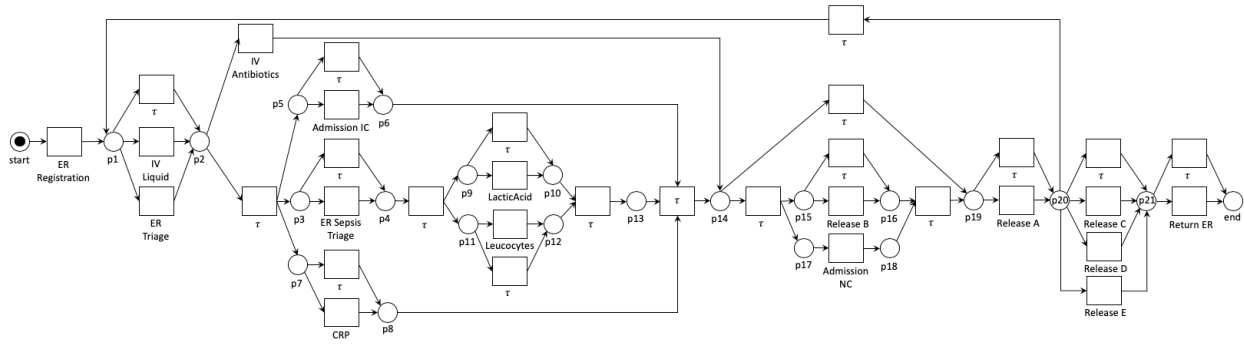


Figure 17. Sepsis Inductive Miner process model.

Miner	Domain	Dataset	Baselines		Our approaches		Over Apprx.	% Approx. Traces	Over Apprx.
			ILP Alignments	extended MEQ Alignments	Automata-based Approach	S-Component Approach			
IM	public	BPIC15 _{2f}	2.019	2.019	2.019	2.071	0.052	5.2%	1
		SEPSIS	0.115	0.115	0.115	0.117	0.002	0.2%	1
	private	PRT6	0.089	0.089	0.089	0.117	0.028	2.7%	1.05
		PRT9	0.378	0.378	t/out	0.391	0.013	0.9%	1.497
SM	public	BPIC12	1.285	1.285	1.285	1.301	0.016	0.8%	2
	private	PRT7	1.398	1.398	1.398	1.410	0.012	1.2%	1

Table 4. Cost comparison and order of approximation for those log-model pairs where S-Components over-approximate

6.4. Threats to validity

A potential threat to validity is the number of threads used in our experiments (16). A different number of threads can lead to different results. For that reason, we repeated our experiments in single-thread mode. The results are reported in Appendix B and are consistent with those obtained by the multi-threaded evaluation.

Another potential threat to validity is the selection of datasets. We decided to use two datasets of real-life log-model pairs from a recent discovery benchmark [32]. These datasets exhibit a wide range of structural characteristics and originate from different industry domains, so they provide a good representation of reality. However, the models discovered by Split Miner did not contain a lot of parallel structures and were thus not highlighting the strengths of the S-Components decomposition. This calls for further experiments with models with a higher degree of parallelism, and more in general, with very large real-life log-model pairs. Such datasets are not publicly available at the time of writing. An alternative, is to use artificial datasets as in [47].

A final threat to validity is posed by the number of methods used for automated process discovery (two). Potentially we could have chosen a larger number of methods. The choice of Split Miner and Inductive Miner was determined by both pragmatic reasons (other methods such as Structured Heuristics Miner return models with duplicate labels which we cannot handle, or led to models for which fitness could not be computed) as well as by the need to test two extreme cases: models with large state spaces versus models with large degrees of parallelism. Moreover,

they are the best performing automated discovery methods according to the benchmark in [32]. So, all considered, they constitute a sufficiently representative set of discovery methods.

7. Conclusion

This paper presented an automata-based technique for conformance checking of process models against event logs. Specifically, the paper showed that the problem of conformance checking can be mapped to that of computing a minimal error-correcting product between an automaton representing the event log (its minimal DAFSA) and an automaton representing the process model (its reachability graph). The resulting product automaton can be used to produce sets of optimal alignments between each trace in the log and a corresponding trace in the model.

The use of a DAFSA to represent the event log allows us to benefit from both prefix and suffix compression of the traces in the log. This is a distinctive feature of the proposal with respect to existing trace alignment techniques, which compute an alignment between each trace in the log and the model, without any reuse across traces. The empirical evaluation reported in the paper shows that this approach outperforms state-of-the-art trace alignment techniques in a clear majority of cases.

The proposed automata-based technique suffers from combinatorial explosion when the process model contains a large number of concurrent branches. To address this shortcoming, we combined the automata-based conformance checking technique with a technique to decompose a process model (specifically a Petri net) into a collection of concurrency-free components, namely S-components. Each of these S-components (which corresponds to an automaton) can be aligned separately against a projected version of the log, in such a way that the alignments can be recomposed into a correct (although not necessarily optimal) alignment. The evaluation showed that this decomposition-based approach achieves lower execution times than the monolithic automata-based approach when the number of S-components is high, in part thanks to the fact that the decomposition-based approach lends itself to parallel computation. The evaluation also showed that the decomposition-based approach computes optimal alignments in the majority of cases. In those model-log pairs where it does not find the optimal (minimal) alignments, the over-approximation is small (one or a handful of moves) and it only occurs for a small percentage of traces (5% or less).

The proposed technique still fails to perform satisfactorily on a handful of the event logs used in the evaluation. Further improvements may be achieved by designing better heuristic functions to guide the A* algorithm.

In this article, we combined S-components decomposition with an automata-based approach to align each S-component against the event log. This combination is natural, since each S-component corresponds to a concurrency-free slice of the process model, which can be seen as an automaton. It is possible however to combine this S-component decomposition approach with existing exact or approximate trace alignment techniques, including the trace alignment techniques of Adriansyah et al. [3] or Van Dongen [5]. An avenue for future work is to explore the relative performance of the S-component decomposition approach with other conformance checking algorithms.

This article focused on the problem of identifying unfitting log behavior. Another avenue for future work is to extend the approach to detect additional model behavior, for example by adapting the ideas proposed in [4] in the context of event structures.

Acknowledgments. This research is partly funded by the Australian Research Council (grant DP180102839) and the Estonian Research Council (grant IUT20-55).

References

- [1] W. M. P. van der Aalst, *Process Mining - Data Science in Action*, Second Edition, Springer, 2016.
- [2] J. Carmona, B. F. van Dongen, A. Solti, M. Weidlich, *Conformance Checking - Relating Processes and Models*, Springer, 2018.
- [3] A. Adriansyah, B. van Dongen, W. van der Aalst, Conformance checking using cost-based fitness analysis, in: *Proc. of EDOC*, IEEE, 2011, pp. 55–64.
- [4] L. García-Bañuelos, N. R. van Beest, M. Dumas, M. La Rosa, W. Mertens, Complete and interpretable conformance checking of business processes, *IEEE Transactions on Software Engineering* 44 (3) (2018) 262–290.
- [5] B. F. van Dongen, Efficiently computing alignments, in: *International Conference on Business Process Management*, Springer, 2018, pp. 197–214.
- [6] A. Augusto, R. Conforti, M. Dumas, M. L. Rosa, F. M. Maggi, A. Marrella, M. Mecella, A. Soo, Automated discovery of process models from event logs: Review and benchmark, *IEEE Trans. Knowl. Data Eng.* 31 (4) (2019) 686–705.

- [7] D. Reißner, R. Conforti, M. Dumas, M. La Rosa, A. Armas-Cervantes, Scalable conformance checking of business processes, in: H. Panetto, C. Debruyne, W. Gaaloul, M. Papazoglou, A. Paschke, C. A. Ardagna, R. Meersman (Eds.), *On the Move to Meaningful Internet Systems. OTM 2017 Conferences*, Springer International Publishing, Cham, 2017, pp. 607–627.
- [8] A. Rozinat, W. van der Aalst, Conformance checking of processes based on monitoring real behavior, *Inf. Syst.* 33 (1) (2008) 64–95.
- [9] A. Alves de Medeiros, Genetic process mining, Ph.D. thesis, TU/e (2006).
- [10] S. vanden Broucke, J. Munoz-Gama, J. Carmona, B. Baesens, J. Vanthienen, Event-based real-time decomposed conformance analysis, in: *Proc. of OTM*, Springer, 2014, pp. 345–363.
- [11] J. Muñoz-Gama, J. Carmona, W. van der Aalst, Single-entry single-exit decomposed conformance checking, *Inf. Syst.* 46 (2014) 102–122.
- [12] M. de Leoni, A. Marrella, Aligning real process executions and prescriptive process models through automated planning, *Expert Systems with Applications* 82 (2017) 162–183.
- [13] M. Nielsen, G. Plotkin, G. Winskel, Petri nets, event structures and domains, part I, *Theoretical Computer Science* 13 (1).
- [14] B. van Dongen, J. Carmona, T. Chatain, F. Taymouri, Aligning modeled and observed behavior: a compromise between complexity and quality, in: *Proc. of CAiSE*, Springer, 2017.
- [15] F. Taymouri, J. Carmona, An evolutionary technique to approximate multiple optimal alignments, in: M. Weske, M. Montali, I. Weber, J. vom Brocke (Eds.), *Business Process Management*, Springer International Publishing, Cham, 2018, pp. 215–232.
- [16] W. M. Van der Aalst, Decomposing petri nets for process mining: A generic approach, *Distributed and Parallel Databases* 31 (4) (2013) 471–507.
- [17] L. Wang, Y. Du, W. Liu, Aligning observed and modelled behaviour based on workflow decomposition, *Enterprise Information Systems* 11 (8) (2017) 1207–1227.
- [18] H. Verbeek, W. M. van der Aalst, Merging alignments for decomposed replay, in: *International Conference on Application and Theory of Petri Nets and Concurrency*, Springer, 2016, pp. 219–239.
- [19] W. Song, X. Xia, H. Jacobsen, P. Zhang, H. Hu, Efficient alignment between event logs and process models, *IEEE Transactions on Services Computing* 10 (1) (2017) 136–149.
- [20] A. Diller, Z: An introduction to formal methods, John Wiley & Sons, Inc., 1990.
- [21] W. M. Van der Aalst, The application of petri nets to workflow management, *journal of circuits, systems, and computers* 8 (01) (1998) 21–66.
- [22] H. M. W. E. Verbeek, T. Basten, W. M. P. v. d. Aalst, Diagnosing Workflow Processes using Woflan, *Comput. J.* 44 (4) (2001) 246–279.
- [23] E. Mayr, An algorithm for the general petri net reachability problem, *SIAM journal on computing* 13 (3) (1984) 441–460.
- [24] R. Lipton, The reachability problem requires exponential space, Research Report 62, Department of Computer Science, Yale University, New Haven, Connecticut.
- [25] T. Murata, Petri nets: Properties, analysis and applications, *Proceedings of the IEEE* 77 (4) (1989) 541–580.
- [26] J. Daciuk, S. Mihov, B. Watson, R. Watson, Incremental construction of minimal acyclic finite-state automata, *Computational linguistics* 26 (1) (2000) 3–16.
- [27] A. Armas-Cervantes, P. Baldan, M. Dumas, L. García-Bañuelos, Diagnosing behavioral differences between business process models: An approach based on event structures, *Information Systems* 56.
- [28] P. Hart, N. Nilsson, B. Raphael, A formal basis for the heuristic determination of minimum cost paths, *IEEE TSSC* 4 (2) (1968) 100–107.
- [29] J. Desel, J. Esparza, *Free choice Petri nets*, Vol. 40, Cambridge university press, 2005.
- [30] A. Adriansyah, B. F. van Dongen, W. M. P. van der Aalst, Conformance checking using cost-based fitness analysis, in: *2011 IEEE 15th International Enterprise Distributed Object Computing Conference*, 2011, pp. 55–64. doi:10.1109/EDOC.2011.12.
- [31] B. F. van Dongen, Efficiently computing alignments, in: F. Daniel, Q. Z. Sheng, H. Motahari (Eds.), *Business Process Management Workshops*, Springer International Publishing, Cham, 2019, pp. 44–55.
- [32] A. Augusto, R. Conforti, M. Dumas, M. La Rosa, F. M. Maggi, A. Marrella, M. Mecella, A. Soo, Automated discovery of process models from event logs: Review and benchmark, *IEEE Transactions on Knowledge and Data Engineering* 31 (4) (2019) 686–705.
- [33] Van Dongen, B.F. (Boudewijn), Bpi challenge 2012 (2012). doi:10.4121/UUID:3926DB30-F712-4394-AEBC-75976070E91F. URL <https://data.4tu.nl/repository/uuid:3926db30-f712-4394-aebc-75976070e91f>
- [34] W. Steeman, Bpi challenge 2013, closed problems (2013). doi:10.4121/UUID:C2C3B154-AB26-4B31-A0E8-8F2350DDAC11. URL <https://data.4tu.nl/repository/uuid:c2c3b154-ab26-4b31-a0e8-8f2350ddac11>
- [35] W. Steeman, Bpi challenge 2013, incidents (2013). doi:10.4121/UUID:500573E6-ACCC-4B0C-9576-AA5468B10CEE. URL <https://data.4tu.nl/repository/uuid:500573e6-cccc-4b0c-9576-aa5468b10cee>
- [36] Van Dongen, B.F. (Boudewijn), Bpi challenge 2014 (2014). doi:10.4121/UUID:C3E5D162-0CFD-4BB0-BD82-AF5268819C35. URL <https://data.4tu.nl/repository/uuid:c3e5d162-0cfd-4bb0-bd82-af5268819c35>
- [37] Van Dongen, B.F. (Boudewijn), Bpi challenge 2015 (2015). doi:10.4121/UUID:31A308EF-C844-48DA-948C-305D167A0EC1. URL <https://data.4tu.nl/repository/uuid:31a308ef-c844-48da-948c-305d167a0ec1>
- [38] Van Dongen, B.F. (Boudewijn), Bpi challenge 2017 (2017). doi:10.4121/UUID:5F3067DF-F10B-45DA-B98B-86AE4C7A310B. URL <https://data.4tu.nl/repository/uuid:5f3067df-f10b-45da-b98b-86ae4c7a310b>
- [39] De Leoni, M. (Massimiliano), Mannhardt, F. (Felix), Road traffic fine management process (2015). doi:10.4121/UUID:270FD440-1057-4FB9-89A9-B699B47990F5. URL <https://data.4tu.nl/repository/uuid:270fd440-1057-4fb9-89a9-b699b47990f5>
- [40] Mannhardt, F. (Felix), Sepsis cases - event log (2016). doi:10.4121/UUID:915D2BFB-7E84-49AD-A286-DC35F063A460. URL <https://data.4tu.nl/repository/uuid:915d2bfb-7e84-49ad-a286-dc35f063a460>
- [41] R. Conforti, M. La Rosa, A. H. ter Hofstede, Filtering out infrequent behavior from business process event logs, *IEEE Transactions on Knowledge and Data Engineering* 29 (2) (2016) 300–314.
- [42] S. J. Leemans, D. Fahland, W. M. van der Aalst, Discovering block-structured process models from event logs-a constructive approach, in: *International conference on applications and theory of Petri nets and concurrency*, Springer, 2013, pp. 311–329.
- [43] A. Augusto, R. Conforti, M. Dumas, M. La Rosa, Split miner: Discovering accurate and simple business process models from event logs, in: *2017 IEEE International Conference on Data Mining (ICDM)*, IEEE, 2017, pp. 1–10.

- [44] A. Augusto, R. Conforti, M. Dumas, M. La Rosa, G. Bruno, Automated discovery of structured process models from event logs: the discover-and-structure approach, *Data and Knowledge Engineering* (to appear).
- [45] S. K. vanden Broucke, J. De Weerd, Fodina: a robust and flexible heuristic process discovery technique, *decision support systems* 100 (2017) 109–118.
- [46] D. Reißner, Public benchmark data-set for conformance checking in process mining (May 2019). doi:10.26188/5cd91d0d3adaa.
URL https://melbourne.figshare.com/articles/Public_benchmark_data-set_for_Conformance_Checking_in_Process_Mining/8081426
- [47] Munoz-Gama, J. (Jorge), 'conformance checking in the large' (bpm 2013) (2013). doi:10.4121/UUID:44C32783-15D0-4DBD-AF8A-78B97BE3DE49.
URL <https://data.4tu.nl/repository/uuid:44c32783-15d0-4dbd-af8a-78b97be3de49>
- [48] J. Esparza, Synthesis rules for petri nets, and how they lead to new results, in: *CONCUR '90*, Vol. 458 of *Lecture notes in Computer Science*, Springer, 1990, pp. 182–198. doi:10.1007/BFb0039060.
URL <https://doi.org/10.1007/BFb0039060>

Appendix A. Complete Cost comparison and order of approximation

Miner	Domain	Dataset	Baselines		Our approaches		Over Apprx.	%Approx. Traces	∅Over Apprx.
			ILP Alignments	extended MEQ Alignments	Automata-based Approach	S-Component Approach			
IM	public	BPIC12	0.871	0.871	0.871	0.871	0	0%	0
		BPIC13 _{cp}	1.461	1.461	1.461	1.461	0	0%	0
		BPIC13 _{inc}	0.839	0.839	0.839	0.839	0	0%	0
		BPIC14 _f	1.937	1.937	t/out	1.937	0	0%	0
		BPIC15 _{1f}	0.503	0.503	t/out	t/out	-	-	-
		BPIC15 _{2f}	2.019	2.019	2.019	2.071	0.052	5.2%	1
		BPIC15 _{3f}	1.699	1.699	1.699	1.699	0	0%	0
		BPIC15 _{4f}	1.137	1.137	1.137	1.137	0	0%	0
		BPIC15 _{5f}	1.198	1.198	1.198	1.198	0	0%	0
		BPIC17 _f	0.832	0.832	0.832	0.832	0	0%	0
		RTFMP	0.057	0.057	0.057	0.057	0	0%	0
		SEPSIS	0.115	0.115	0.115	0.117	0.002	0.2%	1
	private	PRT1	1.427	1.427	1.427	1.427	0	0%	0
		PRT2	t/out	t/out	t/out	t/out	-	-	-
		PRT3	0.231	0.231	0.231	0.231	0	0%	0
		PRT4	1.224	1.224	1.224	1.224	0	0%	0
		PRT6	0.089	0.089	0.089	0.117	0.028	2.7%	1.05
		PRT7	0	0	0	0	0	0%	0
		PRT9	0.378	t/out	0.378	0.391	0.013	0.9%	1.497
		PRT10	0.058	0.058	0.058	0.058	0	0%	0
SM	public	BPIC12	1.285	1.285	1.285	1.301	0.016	0.8%	2
		BPIC13 _{cp}	0.094	0.094	0.094	0.094	0	0%	0
		BPIC13 _{inc}	0.238	0.238	0.238	0.238	0	0%	0
		BPIC14 _f	2.907	t/out	2.907	2.907	0	0%	0
		BPIC15 _{1f}	3.195	3.195	3.195	3.195	0	0%	0
		BPIC15 _{2f}	10.225	10.225	10.225	10.225	0	0%	0
		BPIC15 _{3f}	9.695	9.695	9.695	9.695	0	0%	0
		BPIC15 _{4f}	10.420	10.420	10.420	10.420	0	0%	0
		BPIC15 _{5f}	8.098	8.098	8.098	8.098	0	0%	0
		BPIC17 _f	1.470	1.470	1.470	1.470	0	0%	0
		RTFMP	0.034	0.034	0.034	0.034	0	0%	0
		SEPSIS	4.719	t/out	4.719	4.719	0	0%	0
	private	PRT1	0.293	0.293	0.293	0.293	0	0%	0
		PRT2	8.316	t/out	8.316	8.316	0	0%	0
		PRT3	2.544	2.544	2.544	2.544	0	0%	0
		PRT4	1.907	1.907	1.907	1.907	0	0%	0
		PRT6	1.079	1.079	1.079	1.079	0	0%	0
		PRT7	1.398	1.398	1.398	1.410	0.012	1.2%	1
		PRT9	0.350	t/out	0.350	0.350	0	0%	0
		PRT10	0.105	0.105	0.105	0.105	0	0%	0

Table A.5. Complete cost comparison and order of approximation

Appendix B. Time performance - single threaded

Miner	Domain	Dataset	Baselines		Our Approaches		
			ILP Alignments	extended MEQ Alignments	Automata-based Approach	S-Component Approach	Hybrid Approach
IM	public	BPIC12	125,948	t/out	428,166	160,070	160,070
		BPIC13 _{cp}	295	2,137	330	317	330
		BPIC13 _{inc}	2,040	79,597	24,917	504	504
		BPIC14 _f	98,667	592,238	t/out	9,844	9,844
		BPIC15 _{1f}	3,691	6,015	t/out	t/out	t/out
		BPIC15 _{2f}	19,805	25,185	8,061	16,418	16,418
		BPIC15 _{3f}	31,075	91,996	12,218	69,432	12,218
		BPIC15 _{4f}	12,093	38,816	3,837	8,064	8,064
		BPIC15 _{5f}	8,174	15,553	32,413	18,582	32,413
		BPIC17 _f	22,805	257,705	7,127	8,996	7,127
		RTFMP	3,924	147,135	1,779	1,024	1,024
		SEPSIS	6,964	17,785	58,571	2,984	2,984
	private	PRT1	1,379	12,454	2,527	693	693
		PRT2	t/out	t/out	t/out	t/out	t/out
		PRT3	425	2,175	392	404	392
		PRT4	3,945	22,515	6,069	1,954	6,069
		PRT6	335	1,168	315	330	315
		PRT7	300	2,560	301	323	301
		PRT9	29,538	t/out	68,047	1,937	1,937
		PRT10	970	49,160	350	724	724
SM	public	BPIC12	189,423	t/out	32,035	111,256	32,035
		BPIC13 _{cp}	350	3,481	258	232	258
		BPIC13 _{inc}	1,764	96,106	766	918	766
		BPIC14 _f	40,161	t/out	26,605	31,743	26,605
		BPIC15 _{1f}	3,239	2,941	2,266	2,048	2,266
		BPIC15 _{2f}	9,534	7,025	3,568	3,678	3,568
		BPIC15 _{3f}	7,541	12,926	2,531	2,660	2,531
		BPIC15 _{4f}	7,516	8,220	2,345	2,388	2,345
		BPIC15 _{5f}	9,111	6,303	2,710	2,815	2,710
		BPIC17 _f	28,474	91,585	6,357	8,206	6,357
		RTFMP	3,477	146,871	354	593	354
		SEPSIS	5,355	t/out	1,179	1,219	1,179
	private	PRT1	2,391	66,135	664	809	664
		PRT2	36,539	t/out	18,218	18,531	18,218
		PRT3	365	2,627	332	437	332
		PRT4	7,319	160,196	3,151	6,831	3,151
		PRT6	230	1,005	249	300	249
		PRT7	256	2,256	258	422	258
		PRT9	27,542	t/out	1,472	2,183	1,472
		PRT10	1,263	96,503	328	362	328
Total outperforming:		7	0	23	9	26	
Total second:		8	2	6	23	9	
#Timeouts:		1	8	3	2	2	

Table B.6. Time performance in milliseconds – single-threaded

Appendix C. Recomposing partial alignments is correct

Theorem 5.1 states that the sequence ε_c returned by Alg. 5^{*}($\mathcal{L}, \mathcal{D}, SN$), the modification of Alg. 5 constructing reachability graphs as described in Sect. 5.4, is an alignment of \mathcal{D} to a sound, uniquely-labeled, free-choice workflow net SN . In other words, the projection ε_c onto the left-hand component is trace c , and the projection on the right-hand component is a path through the reachability graph of WN . We prove both properties individually.

Proof of Thm 5.1.1. We show $\lambda(\varepsilon_c \upharpoonright_{\mathcal{D}}) = c$ by induction on the prefixes c' of c in the for-loop in lines 10–39. For the empty prefix c' before the for-loop, $\varepsilon_c = \langle \rangle$. In each iteration of the for-loop with $pos_c \leq |c|$, the prefix c' is extended with $\ell = c(pos_c) \in L$, and the current prefix of ε_c is extended with a synchronization ($lhide, (n, \ell, n'), \perp$) (line 27) or ($match, (n, \ell, n'), (m, \ell, m')$) (line 33). Thus, the proposition holds for both prefixes. The only other extension of the current prefix of ε_c in Alg.5 is with synchronizations ($lhide, \perp, (m, \ell, m')$) in line 18 which do not occur in $\lambda(\varepsilon_c \upharpoonright_{\mathcal{D}})$. \square

Proving Thm 5.1.2 requires some further notation, definitions, and observations on Petri nets.

For a WN, let $\mathcal{C} = \{WN_1, WN_2, \dots, WN_k\}$ be the set of S-Components of WN. By the abuse of notation, let $\mathcal{C}(t)$ be the set of S-components in which t is contained as $WN_i = ((P_i, T_i, F_i, \lambda_i), i_i, o_i) \in \mathcal{C}(t)$ iff $t \in T_i$, for each $t \in T$; sets $\mathcal{C}(p), p \in P_i$, are defined accordingly.

In a sound free-choice net WN, the pre- and post-sets of a transition t (together) cover the same S-component, which follows from WN being covered by S-components [48] and the free-choice structure:

$$\bigcup_{p \in \bullet t} \mathcal{C}(p) = \mathcal{C}(t) = \bigcup_{p \in t \bullet} \mathcal{C}(p). \quad (C.1)$$

In any free-choice net WN with S-components $\{WN_1, WN_2, \dots, WN_k\}$ and reachability graphs $\mathcal{R}(WN_j) = (M^j, A^j, m_0^j, M_f^j), j = 1, \dots, k$ holds:

$$\text{each reachable marking } m \in M^j \text{ has the form } m = [p], p \in P_j \quad (C.2)$$

$$\text{each arc } a \in A^j \text{ has the form } a = ([p], \lambda(t), [p']), p, p' \in P_j, t \in T_j \quad (C.3)$$

Without loss of generality, in a sound, free-choice workflow net $WN = (P, T, F, \lambda, m_0, m_f)$ holds $m_0 = [p_0], p_0 \in P, \bullet p_0 = \emptyset$ and $m_f = \{[p_f]\}, p_f \in P, p_f \bullet = \emptyset$.

Proof of Thm 5.1.2. We have to show that $\varepsilon_c \upharpoonright_{\mathcal{D}}$ corresponds to a path through the \mathcal{R} of WN. Let $\varepsilon_c \upharpoonright_{\mathcal{D}} = (a_1, \dots, a_s)$.

By equation (C.2), each $m_i = ([p^1], \dots, [p^k])$ and for the k S-components of WN. For such a vector $m = ([p^1], \dots, [p^k])$ let, $\widehat{m} = \{p^1, \dots, p^k\}$ be the set of marked places.

We show the proposition by showing that (a) $\widehat{m}_0 = m_0^{WN}$, (b) each $\widehat{m}_i \in M_{\mathcal{R}(WN)}, i = 1, \dots, s'$ is a marking of WN, (c) each $(\widehat{m}_i, \ell_i, \widehat{m}'_i) \in A_{\mathcal{R}(WN)}$ is a step in WN, and (d) $\widehat{m}'_{s'} \in M_f^{WN}$.

Regarding (a), the initial marking of each S-component $j = 1, \dots, k$ is $m_0^j = [p_0]$ as $m_0^{WN} = [p_0]$. Thus, the proposition holds by $m_0 = ([p_0], \dots, [p_0])$ in line 9.

We show (b) and (c) by induction on the length i of the prefixes of ε_c . For $i = 0$, (b) holds for m_0 due to (a), and (c) holds trivially. For $i > 0$, if $\varepsilon_c \upharpoonright_{\mathcal{D}}[i] = \perp$ then there is nothing to show. Otherwise, $\varepsilon_c \upharpoonright_{\mathcal{D}}[i] = (op, a_D, (m_{i-1}, \ell_i, m_i))$ and $m_{i-1} \in A_{\mathcal{R}(WN)}$ by inductive assumption. We have to show: for $([p_{i-1}^1], \dots, [p_{i-1}^k]) = m_{i-1}$ and $([p_i^1], \dots, [p_i^k]) = m_i$, $(\widehat{m}_{i-1}, \ell_i, \widehat{m}_i) \in A_{\mathcal{R}(WN)}$.

If $\ell_i \neq \ell = c(pos_c)$ in line 11, then $\mathcal{C}_\ell \neq \emptyset$, and then (m_{i-1}, ℓ_i, m_i) due to line 18, $m_i = m_{i-1} \blacktriangleright (a_1, \dots, a_k)$, and $lab_x = sync_x = \mathcal{C}(t)$ for some transition $t \in T, \lambda(t) = \ell_i = x$ (by lines 15,16). If there was no such t , then ε_c is due to line 40 and the proposition holds by Lem. 4.2.

Because WN is uniquely labeled, t is unique. By line 14, $([p_{i-1}^j], \ell_i, [p_i^j]) \in A_{\mathcal{R}}^j$ for each $j \in \mathcal{C}(t)$. Due to (C.1), the preset of t is marked, $\bullet t = \{p_{i-1}^j \mid j \in \mathcal{C}(t)\} \subseteq \widehat{m}_{i-1}$, and t is enabled in \widehat{m}_{i-1} . Firing t yields the successor marking $m^* = (\widehat{m}_{i-1} \setminus \bullet t) \cup t \bullet = (\widehat{m}_{i-1} \setminus \{p_{i-1}^j \mid j \in \mathcal{C}(t)\}) \cup \{p_i^j \mid j \in \mathcal{C}(t)\}$ by (C.1). By construction of (a_1, \dots, a_k) in line 17 from $sync_x = \mathcal{C}(t)$, we can rewrite $m^* = (\widehat{m}_{i-1} \setminus \{p_{i-1}^j \mid a_j \neq \perp\}) \cup \{p_i^j \mid a_j \neq \perp\}$ as Alg. 1* ensures transition effects are uniquely identified by their extended labels (see Sect. 5.4). By line 18, and the definition of \blacktriangleright , $m^* = \widehat{m}_i$. Thus, $(\widehat{m}_{i-1} \setminus \bullet t) \cup t \bullet = \widehat{m}_i$ and propositions b and c hold.

If $\ell_i = \ell = c(pos_c)$ then (m_{i-1}, ℓ_i, m_i) due to line 33 and a similar reasoning as above holds as there exists a unique transition t with $\lambda(t) = \ell_i$ and $([p_{i-1}^j], \ell_i, [p_i^j]) \in A_{\mathcal{R}}^j$ with $p_{i-1}^j \in \widehat{m}_{i-1}$ for each $j \in \mathcal{C}(t)$.

To prove (d), we know $m_f^{WN} = \{[p_f]\}$, by N having a unique final place p_f . Thus, for $m'_{s'} = ([p_{s'}^1], \dots, [p_{s'}^k])$, $p_{s'}^j = p_f$ has to hold for all $j = 1, \dots, k$. Suppose that for the recomposed alignment, there exists $j \in \{1, \dots, k\}$ where in $m'_{s'}, [p_{s'}^j] \neq [p_f]$. Each ε_j calculated in line 5 of Alg. 5* is an alignment. Thus, the path $\varepsilon_j^{a_{\mathcal{R}}} \upharpoonright_{L_j} = (a_1^j, \dots, a_{s_j}^j)$

through $\mathcal{R}(WN_j)$ ends in the final place $a_{s_j}^j = (m^j, \ell_j, [p_f])$, and thus $\mathcal{R}(WN_j)$ has further arcs from $[p_{s'}^j]$ to $[p_f]$ that should have been considered by Alg. 5*. Case distinction:

(i) For all $j = 1, \dots, k$, $[p_{s'}^j] \neq [p_f]$ with two possible cases:

(i-a) There exists some $t \in T$ of WN with $\widehat{m'_{s'}} \supseteq \bullet t$ and $\lambda(t) = x$. Then either $\text{sync}_x = \text{lab}_x$ in line 16 of Alg. 5* and a synchronization with arc $(m'_{s'}, x, m'')$ would have been added to ε_c by the arguments for (c) given above. Or $x = \ell = c(\text{pos}_c), \text{pos}_c < |c|$ and a corresponding synchronziation would have been added in line 33 of Alg.5. Both cases contradict the algorithm.

(i-b) There exists no $t \in T$ with $\widehat{m'_{s'}} \supseteq \bullet t$. But then $m'_{s'}$ is a deadlock contradicting WN being sound.

(ii) There exist j, r , $[p_{s'}^j] \neq [p_f]$ and $[p_{s'}^r] = [p_f]$. By (b) and (c), $\widehat{m'_{s'}} \subseteq \{p_f, p_{s'}^j\}$ is a reachable marking of WN which contradicts WN being sound.

□